ROSAT X-Ray Colors and Emission Mechanisms in Early-Type Galaxies

Jimmy A. Irwin – University of Virginia
Craig L. Sarazin - University of Virginia

Citation of published version:

Bregman, J., Irwin, J. (1998): ROSAT X-Ray Colors and Emission Mechanisms in Early-Type Galaxies. *The Astrophysical Journal*, 499(2). DOI: 10.1086/305666

THE ASTROPHYSICAL JOURNAL, 499:650–669, 1998 June 1

ROSAT X-RAY COLORS AND EMISSION MECHANISMS IN EARLY-TYPE GALAXIES

JIMMY A. IRWIN AND CRAIG L. SARAZIN
Department of Astronomy, University of Virginia, P.O. Box 3818, Charlottesville, VA 22903-0818; jai7e@virginia.edu, cls7i@virginia.edu
Received 1997 August 11; accepted 1998 January 13

ABSTRACT

The X-ray colors and X-ray–to–optical luminosity ratios (L_X/L_B) of 61 early-type galaxies observed with the *ROSAT* PSPC are determined. The colors indicate that the X-ray spectral properties of galaxies vary as a function of L_X/L_B. The brightest X-ray galaxies have colors that are consistent with thermal emission from hot gas with roughly the same metallicity of 50% solar. The spatial variation of the colors indicates that the gas temperature in these galaxies increases radially. Galaxies with medium L_X/L_B also have spectral properties consistent with emission from hot gas. If a simple one-component thermal model is assumed to describe the 0.1–2.0 keV X-ray emission in these galaxies, then one possible explanation for the progressive decrease in L_X/L_B among galaxies of this class could be the progressive decrease in metal abundance of the X-ray–emitting gas contained by the galaxies. However, stellar X-ray emission may become a complicating factor for the fainter galaxies in this medium-L_X/L_B class.

Galaxies with the lowest L_X/L_B values appear to be lacking a hot interstellar component. Their X-ray colors are consistent with those derived from the bulges of the spiral galaxies M31 and NGC 1291. In M31, the X-ray emission is resolved into discrete sources and is apparently due primarily to low-mass X-ray binaries (LMXBs). We therefore suggest that the bulk of the X-ray emission in the faintest elliptical galaxies is also due to LMXBs. Previously, the X-ray spectra of X-ray–faint galaxies had been found to be described by a hard component, which was attributed to LMXB emission, and a very soft component of unknown origin. We show that the very soft component also likely results from LMXBs, as a very soft component is seen in the X-ray spectra of the nearby LMXB Her X-1 and LMXBs in the bulge of M31. If the X-ray emission in X-ray–faint galaxies is primarily from stellar sources, then a range in L_X/L_B among these galaxies suggests that the stellar X-ray luminosity does not scale with optical luminosity, at least for galaxies of low optical luminosities. This could be the result of a decrease in the proportion of LMXBs with decreasing optical luminosity and/or the effects of fluctuations in the small number of LMXBs expected.

Subject headings: galaxies: abundances — galaxies: elliptical and lenticular, cD — galaxies: halos — galaxies: ISM — X-rays: galaxies — X-rays: ISM

1. INTRODUCTION

One surprising fact uncovered by the *Einstein Observatory* was that elliptical and S0 galaxies are relatively bright, extended X-ray sources (e.g., Forman et al. 1979; Forman, Jones, & Tucker 1985; Trinchieri & Fabbiano 1985). It soon was established that the source of these X-rays was thermal emission from hot ($\sim$1 keV), diffuse interstellar gas, at least for the brighter X-ray early-type galaxies. However, several unsolved problems still remain concerning the X-ray emission from elliptical and S0 galaxies. Although there is a strong correlation between the X-ray and blue luminosities in these systems, the X-ray luminosity can vary by as much as a factor of 50–100 among galaxies with the same blue luminosity (Canizares, Fabbiano, & Trinchieri 1987; Fabbiano, Kim, & Trinchieri 1992).

Elliptical and S0 galaxies with a low X-ray–to–blue luminosity ratio (L_X/L_B) also have different spectral characteristics than their X-ray–bright (high-L_X/L_B) counterparts. From *Einstein* observations, Kim, Fabbiano, & Trinchieri (1992) found that the galaxies with the lowest L_X/L_B exhibited an excess of very soft X-ray emission. *ROSAT* position sensitive proportional counter (PSPC) observations of several X-ray–faint galaxies have confirmed that the X-ray emission in such galaxies is not characterized by emission from hot, metal-enriched gas with a temperature of $\sim$1 keV; a two-component model, in which one component has a temperature around 0.2 keV and the other has a temperature greater than a few keV, provides a better fit (Fabbiano, Kim, & Trinchieri 1994; Pellegrini 1994). This result was confirmed by an *ASCA* observation of NGC 4382 (Kim et al. 1996). The source of the soft $\sim$0.2 keV emission has been postulated to be RS CVn binary systems, M-star coronae, supersoft sources, or a low-temperature interstellar medium (ISM), although none of these mechanisms seems to be entirely responsible for the soft X-ray emission (Pellegrini & Fabbiano 1994). The hard component is thought to be emission from accreting compact X-ray binaries; this is the dominant X-ray component in most spiral galaxies (Trinchieri & Fabbiano 1985).

It is difficult to do detailed spectral modeling of these low-L_X/L_B systems because of their low X-ray count rates, even for the closest and brightest examples. Instead, in this paper we will analyze the broadband X-ray "colors" of elliptical and S0 galaxies. These "colors" are the ratios of the counts in three X-ray bands. Whereas conventional spectral fitting requires a minimum of about 1000 counts to constrain reasonably the parameters of the model, only about 100 counts are needed to determine the X-ray colors. This allows much fainter X-ray galaxies to be analyzed and compared to brighter galaxies, leading to a more comprehensive investigation into the X-ray properties of early-type galaxies. A similar technique of determining colors was used to study a large sample of X-ray galaxies with *Einstein* data by Kim et al. (1992). In this paper, we will determine the X-ray colors of early-type galaxies observed with the

TABLE 1

GALAXY SAMPLE

Galaxy	m_B^0	D (Mpc)	$r_{\rm eff}$ (kpc)	$N_{\rm H}$ (10^{20} cm^{-2})
NGC 507	12.13	115.6	29.9	5.42
NGC 524	11.17	48.2	11.6	4.61
NGC 533	12.22	101.0	22.3	3.25
NGC 596	12.13	30.0	4.0	3.53
NGC 720	11.13	41.0	7.2	1.42
NGC 1199	12.23	46.0	6.2	4.29
NGC 1316	9.40	28.4	11.1	2.06
NGC 1332	11.21	39.8	5.4	2.20
NGC 1344	11.24	28.4	3.7	1.18
NGC 1380	10.92	28.4	5.4	1.27
NGC 1381	12.46	28.4	1.6	1.32
NGC 1387	11.70	28.4	2.9	1.36
NGC 1395	10.55	39.8	9.4	1.74
NGC 1399	10.44	28.4	5.6	1.36
NGC 1400	11.89	39.8	5.7	4.97
NGC 1404	10.98	28.4	3.3	1.39
NGC 1407	10.71	39.8	13.6	5.17
NGC 1427	11.81	28.4	4.2	1.38
NGC 1549	10.68	24.2	5.3	1.93
NGC 1553	10.26	24.2	7.7	1.93
NGC 2300	11.77	64.7	9.9	5.88
NGC 3091	11.96	81.7	13.0	4.27
NGC 3115	9.74	20.4	3.2	4.43
NGC 3193	11.73	49.2	6.4	2.12
NGC 3585	10.64	23.5	4.1	5.45
NGC 3607	10.79	39.8	8.4	1.45
NGC 3608	11.69	39.8	6.5	1.45
NGC 3610	11.54	42.7	3.2	0.72
NGC 3640	11.19	45.7	7.1	4.38
NGC 3665	11.69	48.6	6.7	2.08
NGC 4125	10.67	39.7	11.3	1.79
NGC 4261	11.36	55.7	9.7	1.59
NGC 4291	12.25	60.6	5.1	3.22
NGC 4365	10.49	26.6	6.4	1.60
NGC 4371	11.62	26.6	3.0	2.52
NGC 4374	10.01	26.6	6.6	2.78
NGC 4382	9.99	26.6	7.0	2.70
NGC 4406	9.74	26.6	13.4	2.75
NGC 4472	9.33	26.6	13.4	1.64
NGC 4474	12.34	26.6	2.7	2.65
NGC 4477	11.30	26.6	4.9	2.70
NGC 4526	10.53	26.6	5.7	1.61
NGC 4550	12.36	26.6	1.9	2.50
NGC 4552	10.57	26.6	3.8	2.50
NGC 4636	10.43	26.6	11.4	1.91
NGC 4638	12.06	26.6	2.3	2.39
NGC 4649	9.70	26.6	8.9	2.40
NGC 4697	10.07	15.8	5.5	2.09
NGC 4880	12.35	23.6	2.0	2.25
NGC 5044	11.67	59.6	22.8	4.94
NGC 5102	9.99	5.3	0.6	4.73
IC 4296	11.42	75.4	15.1	4.22
IC 4329	11.97	77.9	19.7	4.39
NGC 5322	11.04	33.2	5.4	1.87
NGC 5353	11.98	56.7	4.0	1.02
NGC 5846	10.91	46.7	14.2	4.19
NGC 5866	10.83	23.0	4.5	1.48
ESO 185−54	11.90	91.5	11.6	5.85
NGC 7144	11.68	36.8	5.7	1.78
NGC 7619	11.93	71.6	12.8	4.98
NGC 7626	12.06	71.6	13.4	4.98

ROSAT PSPC. The increased sensitivity of *ROSAT* over *Einstein* allows a larger sample to be analyzed and the X-ray colors to be determined more accurately. In addition to integrated X-ray colors, we also derive the X-ray colors as a function of galactocentric radius to explore the variation of X-ray emission with position. If the emission mechanisms are different between X-ray–faint and X-ray–bright elliptical and S0 galaxies, the integrated colors and color profiles should shed some light on this difference.

This paper is organized as follows. In § 2, we define our galaxy sample and give the relevant properties of the galaxies, and in § 3, we discuss the data analysis. The X-ray luminosities and X-ray–to–optical luminosity ratios in hard and soft bands are discussed in § 4. The integrated X-ray colors of the galaxies are presented in § 5 and are compared to simple models. The radial profiles of the X-ray colors are given in § 6. In § 7, we discuss a number of different mechanisms for the X-ray emission of elliptical galaxies of varying X-ray–to–optical luminosities. We show that the very soft component in X-ray–faint galaxies is unlikely to be due to stellar sources other than low-mass X-ray binaries (LMXBs) or a warm ISM in § 8. Finally, our conclusions are summarized in § 9.

2. GALAXY SAMPLE

In order to create an unbiased galaxy sample, we screened all of the galaxies in the Third Revised Catalog of Galaxies (de Vaucouleurs et al. 1991) according to de Vaucouleurs T-type ($T \leq -1$) and corrected blue apparent magnitude ($m_B^0 \leq 12.5$). Using HEASARC BROWSE, we determined which galaxies were observed with the *ROSAT* PSPC and were available in the public archive. Since both the sensitivity and resolution of the PSPC decrease appreciably outside the rib support structure, we only include galaxies that are contained within the inner edge of the rib ($\lesssim 18'$). Furthermore, we excluded all galaxies with Galactic column densities above 6×10^{20} cm^{-2}, since soft X-rays are very heavily absorbed at high hydrogen column densities. We excluded galaxies that are at the center of rich clusters, since the X-ray emission from these galaxies is contaminated by emission from hot intracluster gas known to be present in such systems. Finally, galaxies deeply buried in the X-ray halo of another bright galaxy, unresolved from another X-ray source, whose X-ray emission was clearly point-like, or that contained an active galactic nucleus according to the Catalogue of Quasars and Active Nuclei (Veron-Cetty & Veron 1996) were excluded. These selection criteria yielded a total of 61 galaxies, whose properties are listed in Table 1. The values for the blue total apparent magnitude, m_B^0, were taken from de Vaucouleurs et al. (1991). The Galactic hydrogen column density for each galaxy is from Stark et al. (1992). The distances to the galaxies are also listed in Table 1. For most of the galaxies, distances were taken from Faber et al. (1989); the remaining distances were taken from Tully (1988). The sole exception was ESO 185−54, which did not appear in either of the above sources. Its distance was taken from Sadler, Jenkins, & Kotanyi (1989). We have assumed a Hubble constant of $H_0 = 50$ km s^{-1} Mpc^{-1}.

3. DATA REDUCTION

All of the data were initially processed using Snowden's (1995) routines in order to correct for particle and scattered solar X-ray background and for exposure and vignetting. Periods of high background due to charged particles were removed by filtering the data such that all time intervals with a master veto rate above 170 counts s^{-1} were excluded. For each data set, three images were created by combining pairs of the seven energy band images produced by the Snowden (1995) routines as follows: R1L + R2 (approximately 0.11–0.41 keV), R4 + R5 (approximately

0.52–0.90 keV), and R6 + R7 (approximately 0.91–2.02 keV). Snowden's R3 band is located in the carbon absorption edge of the detector, is poorly calibrated, and contains little independent spectral information. Nearly all of the data were taken in the post–gain change mode (1991 October 11). However, any data taken before the gain change were analyzed in the low-gain bandpass (R1L) for consistency.

For each of the three energy bands, counts were extracted from concentric annular apertures 30″ in width centered on the peak of X-ray emission for each galaxy. Unrelated X-ray sources within the field of view were identified by eye and removed from the data. In most cases, background counts were obtained from an annular region 30′–40′ in extent and were normalized to and subtracted from each source. After subtracting background, the radial surface brightness profile of the galaxies at large radii fluctuated around zero. This provides evidence that the Snowden (1995) routines do a good job of correcting for exposure, vignetting, and non–X-ray background. In cases where the galaxy of interest was on the outskirts of another galactic X-ray halo, a local background had to be carefully chosen. Again, a surface brightness profile that fluctuated around zero at large distances from the source confirmed the suitability of our background region selection.

Next, we define our two X-ray colors as

$$\mathrm{C21} = \frac{\text{counts in 0.52–0.90 keV band}}{\text{counts in 0.11–0.41 keV band}}, \quad (1)$$

and

$$\mathrm{C32} = \frac{\text{counts in 0.91–2.02 keV band}}{\text{counts in 0.52–0.90 keV band}}. \quad (2)$$

Although similar in spirit to the X-ray colors used by Kim et al. (1992) for *Einstein* data, the colors in these two studies are not directly comparable because of the different photon energy bandpasses and different responses of *Einstein* and *ROSAT*.

For a given emission spectrum, the observed C21 (and, to a lesser extent, C32) color depends significantly on the amount of absorption due to Galactic hydrogen along the line of sight to the galaxy. We developed a technique to correct the colors for absorption, based on the detailed spectral response of the *ROSAT* PSPC. To calibrate the absorption corrections, we first determined the emitted colors (C21 and C32) and the observed colors (C21* and C32*) for an extensive grid of Raymond-Smith (1977) thermal models with varying abundances (ranging from 20% to 100% of solar) and temperatures (ranging from 0.2 to 1.5 keV) and subject to different values for the amount of foreground absorption. The absorbing hydrogen columns considered ranged from $N_{\mathrm{H}} = (0.6\text{–}6) \times 10^{20}$ cm^{-2}; the upper limit corresponds to the upper limit allowed for inclusion in our sample (§ 2). The spectral models were folded through the spectral response of the PSPC using the XSPEC program. We assumed that the unabsorbed colors (C21, C32) could be related to the absorbed colors (C21*, C32*) through relations of the form

$$\ln \mathrm{C21} = \ln \mathrm{C21}^* - A_1(N_{\mathrm{H}}) \left(\frac{N_{\mathrm{H}}}{10^{21}\ \mathrm{cm}^{-2}} \right) + B_1(N_{\mathrm{H}}) \left(\frac{N_{\mathrm{H}}}{10^{21}\ \mathrm{cm}^{-2}} \right) \ln \mathrm{C21}^*, \quad (3)$$

$$\ln \mathrm{C32} = \ln \mathrm{C32}^* - A_2(N_{\mathrm{H}}) \left(\frac{N_{\mathrm{H}}}{10^{21}\ \mathrm{cm}^{-2}} \right), \quad (4)$$

where $A_1(N_{\mathrm{H}})$, $B_1(N_{\mathrm{H}})$, and $A_2(N_{\mathrm{H}})$ are functions of the Galactic column density, N_{H}. In equations (3) and (4), the terms with the coefficients A_1 and A_2 would represent simple exponential absorption if the spectral bands used were infinitely narrow. The term with the coefficient B_1 includes the effect of the spectral distribution of photons within the bands (as parameterized by the color) on the effective optical depth. For the harder C32 color, this additional correction was unnecessary. The absorbed colors from our grid of spectral models and absorptions were compared to those expected from the correction equations (3) and (4). A number of simple forms for the correction coefficient functions A_1, A_2, and B_1 were tried. Empirically, the following functions were found to work well. Once the form of the functions was established, the best-fit values were determined by least-squares fitting to the emitted colors. The resulting correction coefficient functions were

$$A_1(N_{\mathrm{H}}) = 4.57 \left(\frac{N_{\mathrm{H}}}{10^{21}\ \mathrm{cm}^{-2}} \right)^{-0.30}, \quad (5)$$

$$B_1(N_{\mathrm{H}}) = \log \left[3.85 \left(\frac{N_{\mathrm{H}}}{10^{21}\ \mathrm{cm}^{-2}} \right) - 0.21 \right], \quad (6)$$

and

$$A_2 = 0.21. \quad (7)$$

This empirically determined relation was quite effective in correcting the colors for absorption, producing only a 6% root mean square (rms) error in C21 and a 2% rms error in C32 when comparing the absorption-corrected colors to the original unabsorbed colors derived from the spectral models. The rms errors became substantially larger when models with hydrogen column densities greater than 6×10^{20} cm^{-2} were included in the calculation of the correction coefficient functions. It is for this reason that we have excluded all galaxies with column densities above 6×10^{20} cm^{-2} from our sample. For the remainder of this paper, we will refer to the absorption-corrected colors as C21 and C32.

One of the aims of this paper is to study the differing X-ray emission mechanisms in galaxies with differing X-ray luminosities. X-ray luminosities from the *Einstein Observatory* are available for many of our galaxies. However, for consistency with the spectral properties derived from the *ROSAT* PSPC data, we also derived X-ray luminosities from the same data. The X-ray luminosity, L_{X}, of each galaxy was determined for band 1 (0.11–0.41 keV; the "soft" [*s*] band) and for bands 2 and 3 combined (0.52–2.02 keV; the "hard" [*h*] band). The count rates for these bands were converted to physical fluxes and luminosities assuming that the emission spectrum was a Raymond-Smith thermal model with a temperature of 0.8 keV and an abundance of 0.5 solar, using separate model normalizations for hard and soft bands. The fluxes are not strongly dependent on the emission spectrum assumed. The fluxes were corrected for intervening absorption, based on the Galactic hydrogen column toward each galaxy (Table 1). For consistency, the luminosities were all determined for a circular aperture whose radius was five optical effective radii. The effective radius of each galaxy, r_{eff}, which contains one-half of the projected optical luminosity of the galaxy, was taken from

de Vaucouleurs et al. (1991) and is listed in Table 1. Unrelated X-ray sources that fell within the extraction region were removed.

The X-ray luminosities for both bands are listed in Table 2. Some of the galaxies were not detected in one or both of the bands. For these, Table 2 lists the 1 σ confidence upper limit on the X-ray luminosity, preceded by the symbol "$<$." We also determined the blue optical luminosities, L_B, of the galaxies from their magnitudes and distances in Table 1. The X-ray–to–optical luminosity ratios, L_X/L_B, are also listed in Table 2 for each of the two X-ray bands.

The galaxies were grouped into four luminosity classes by

TABLE 2

X-RAY PROPERTIES

Galaxy	log (L_X^h) (ergs s^{-1})	log (L_X^s) (ergs s^{-1})	Group	log (L_X^h/L_B) (ergs s^{-1} $L_{B,\odot}^{-1}$)	log (L_X^s/L_B) (ergs s^{-1} $L_{B,\odot}^{-1}$)	C21	C32
NGC 507	42.90	42.40	4	31.43	30.93	0.45	1.72
NGC 524	40.98	40.50	2	29.89	29.41	0.73	0.75
NGC 533	42.35	41.96	4	31.03	30.64	0.40	1.56
NGC 596	$<$39.24	$<$39.91	1	$<$28.95	$<$29.61	...	...
NGC 720	41.17	40.88	3	30.20	29.91	0.43	0.80
NGC 1199	39.60	$<$40.10	1	28.97	$<$29.47	...	...
NGC 1316	41.11	41.12	2	29.77	29.78	0.30	0.94
NGC 1332	40.91	40.75	2	29.99	29.84	0.36	0.87
NGC 1344	39.49	$<$39.28	1	28.88	$<$28.67	...	...
NGC 1380	40.31	40.32	1	29.58	29.58	0.27	0.69
NGC 1381	$<$38.68	$<$38.98	1	$<$28.57	$<$28.86	...	...
NGC 1387	40.60	40.48	3	30.17	30.05	0.37	0.68
NGC 1395	41.18	40.96	3	30.00	29.79	0.35	1.08
NGC 1399	41.68	41.25	4	30.75	30.33	0.36	2.00
NGC 1400	40.53	40.07	2	29.89	29.43	0.50	0.70
NGC 1404	41.37	40.92	4	30.66	30.21	0.66	0.85
NGC 1407	41.45	40.92	3	30.34	29.81	0.98	1.05
NGC 1427	39.81	39.57	1	29.43	29.19	0.19	2.36
NGC 1549	40.06	40.59	1	29.37	29.90	0.07	0.84
NGC 1553	40.64	40.96	2	29.78	30.10	0.11	1.03
NGC 2300	41.58	40.75	4	30.47	29.64	1.02	0.81
NGC 3091	41.82	41.41	4	30.58	30.17	0.74	1.05
NGC 3115	39.94	39.82	1	29.02	28.90	0.21	1.34
NGC 3193	40.42	40.63	1	29.54	29.74	0.22	0.77
NGC 3585	39.94	$<$39.98	1	29.25	$<$29.29	...	...
NGC 3607	40.89	40.86	2	29.81	29.78	0.27	0.74
NGC 3608	40.50	40.45	2	29.78	29.73	0.27	0.73
NGC 3610	39.82	40.11	1	28.98	29.27	0.12	1.23
NGC 3640	40.38	40.72	1	29.34	29.68	0.11	0.79
NGC 3665	40.80	40.62	2	29.91	29.73	0.42	0.73
NGC 4125	41.02	41.13	2	29.90	30.01	0.22	0.50
NGC 4261	41.49	41.18	3	30.35	30.04	0.44	1.14
NGC 4291	41.34	41.14	4	30.48	30.28	0.38	0.82
NGC 4365	40.40	40.54	1	29.55	29.69	0.25	1.00
NGC 4371	39.93	$<$39.66	1	29.53	$<$29.26	...	...
NGC 4374	41.07	40.81	3	30.03	29.77	0.39	1.01
NGC 4382	40.56	40.78	1	29.51	29.73	0.20	0.53
NGC 4406	42.08	41.63	4	30.93	30.48	0.44	1.26
NGC 4472	41.87	41.31	4	30.55	29.99	0.65	1.56
NGC 4474	$<$39.12	$<$39.61	1	$<$29.01	$<$29.50	...	...
NGC 4477	40.40	40.63	2	29.87	30.10	0.16	0.61
NGC 4526	40.03	40.31	1	29.19	29.48	0.15	0.78
NGC 4550	$<$38.89	$<$39.37	1	$<$28.78	$<$29.27	...	...
NGC 4552	40.92	40.64	3	30.10	29.82	0.42	1.11
NGC 4636	41.89	41.43	4	31.01	30.56	0.66	0.92
NGC 4638	$<$38.75	$<$39.41	1	$<$28.53	$<$29.19	...	...
NGC 4649	41.50	41.06	3	30.33	29.89	0.62	1.19
NGC 4697	40.11	40.41	1	29.55	29.84	0.17	0.83
NGC 4880	$<$38.72	$<$39.33	1	$<$28.72	$<$29.33	...	...
NGC 5044	43.00	42.56	4	31.92	31.48	0.47	1.50
NGC 5102	37.90	38.89	1	28.26	29.24	0.05	0.78
IC 4296	41.79	41.30	4	30.41	29.92	0.42	1.08
IC 4329	42.10	41.59	4	30.91	30.40	0.39	1.51
NGC 5322	40.08	40.59	1	29.26	29.76	0.10	0.93
NGC 5353	41.03	40.83	3	30.12	29.92	0.30	0.92
NGC 5846	42.07	41.56	4	30.90	30.39	0.60	0.93
NGC 5866	40.04	40.45	1	29.46	29.86	0.15	0.84
ESO 185$-$54	41.52	$<$41.18	3	30.17	$<$29.82	...	...
NGC 7144	39.85	40.11	1	29.19	29.46	0.15	0.94
NGC 7619	41.83	41.40	4	30.70	30.27	0.80	1.10
NGC 7626	41.34	40.74	3	30.26	29.66	0.68	0.96

NOTE.—Values preceded by the symbol "$<$" are 1 σ confidence upper limits.

their 0.52–2.02 keV X-ray–to–blue luminosity ratio (L_X^h/L_B). We have followed the convention of Kim et al. (1992) of labeling the X-ray faintest galaxies as group 1 and the X-ray brightest galaxies as group 4, although the boundaries of the four groups differ from theirs. Group 4 galaxies have log $(L_X^h/L_B) \geq 30.4$, group 3 galaxies have $30.0 \leq \log (L_X^h/L_B) < 30.4$, group 2 galaxies have $29.7 \leq \log (L_X^h/L_B) < 30.0$, and group 1 galaxies have $\log (L_X^h/L_B) < 29.7$. These boundaries were chosen so that each group contained roughly the same number of galaxies and, as will be shown below, the same general spectral characteristics. The average properties of the galaxies in our sample within each of these groups are listed in Table 3. For each property, the number given is the mean value and the standard deviation within the group (rather than the error of the mean). The standard deviation is useful as a representation of the scatter in the property among the members of the group.

4. X-RAY/OPTICAL LUMINOSITY RELATION FOR SOFT AND HARD X-RAY BANDS

The hard-band X-ray luminosities or upper limits from Table 2 are plotted as a function of the optical luminosity in Figure 1. Using all of the galaxies in the sample, we found that the unweighted best-fit relation between the hard-band X-ray luminosity (L_X^h) and the optical luminosity was $L_X^h \propto L_B^{2.70\pm0.20}$. Galaxies with only upper limits on their X-ray luminosity were included in the fit, using the parametric EM algorithm within the survival analysis package ASURV (Isobe, Feigelson, & Nelson 1986). This is not an unbiased determination of the X-ray luminosities of optically selected elliptical galaxies because of the unknown selection function associated with *ROSAT* PSPC observations of the galaxies. Still, our relation is consistent with the White & Davis (1997) result, once they excluded dwarf elliptical galaxies and M32. M32 appears as a point source in the *ROSAT* high-resolution imager and most likely contains a small number of X-ray binaries or a micro–active galactic nucleus at its center (Eskridge, White, & Davis 1996). The dispersion in our L_X^h versus L_B relation was 0.55 dex.

Several of the most luminous X-ray galaxies sit at the centers of groups of galaxies and are likely to have their X-ray emission enhanced by group gas. Six of the galaxies in our sample that are located at the centers of groups have integrated X-ray colors distinctly different from the rest of the group 4 galaxies, as will be shown below (§ 5, Fig. 4). These six galaxies are listed in Table 4, which also gives some of their X-ray properties. They are also indicated by open squares in Figure 1. If we remove these six galaxies, we

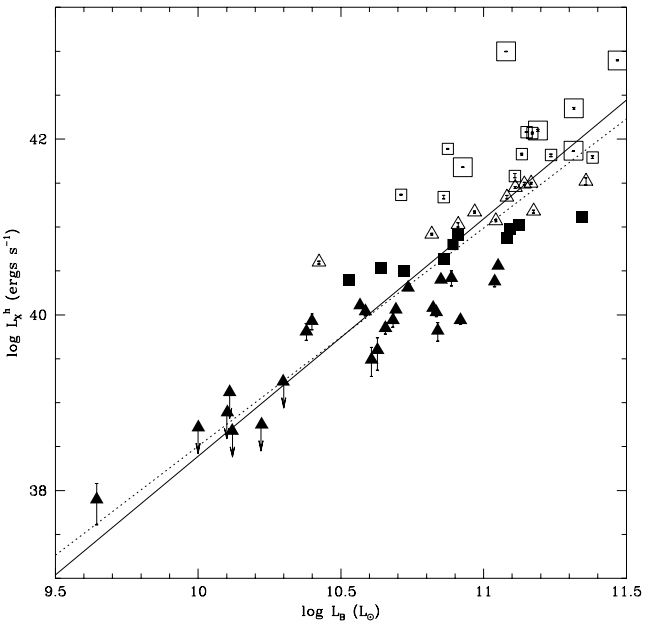

FIG. 1.—Logarithm of the hard-band (0.52–2.02 keV) X-ray luminosity, L_X^h, vs. the logarithm of the blue optical luminosity, L_B, for all of the galaxies in the sample. Group 1, 2, 3, and 4 galaxies are denoted by filled triangles, filled squares, open triangles, and open squares, respectively. Symbols with one-sided vertical arrows are upper limits. The error bars or upper limits on the X-ray luminosity are 1 σ. The six group 4 galaxies located at the centers of groups (Table 4) are shown as large open squares. The best-fit power-law relation is $L_X^h \propto L_B^{2.70\pm0.20}$ if all galaxies are included (*solid line*) and $L_X^h \propto L_B^{2.48\pm0.19}$ if the six group 4 galaxies located in the centers of groups are excluded (*dotted line*).

TABLE 3

AVERAGE X-RAY PROPERTIES FOR LUMINOSITY GROUPS

Parameter	Group 1	Group 2	Group 3	Group 4
Range in log (L_X^h/L_B).....	<29.7	29.7–30.0	30.0–30.4	> 30.4
$\langle$C21$\rangle$	0.16 ± 0.06	0.33 ± 0.17	0.50 ± 0.20	0.56 ± 0.18
$\langle$C32$\rangle$	0.99 ± 0.41	0.76 ± 0.15	0.99 ± 0.15	1.24 ± 0.36
$\langle L_X^h \rangle$ (ergs s^{-1}).....	$(1.3 \pm 0.9) \times 10^{40}$	$(6.9 \pm 3.3) \times 10^{40}$	$(1.9 \pm 1.0) \times 10^{41}$	$(1.9 \pm 2.8) \times 10^{42}$
$\langle L_X^s \rangle$ (ergs s^{-1}).....	$(2.7 \pm 1.7) \times 10^{40}$	$(6.4 \pm 4.1) \times 10^{40}$	$(7.8 \pm 3.4) \times 10^{40}$	$(4.9 \pm 8.6) \times 10^{41}$
$\langle L_B \rangle$ ($L_{B,\odot}$)	$(5.8 \pm 2.8) \times 10^{10}$	$(9.5 \pm 5.3) \times 10^{10}$	$(1.2 \pm 0.5) \times 10^{11}$	$(1.5 \pm 0.7) \times 10^{11}$

TABLE 4

GALAXIES AT THE CENTERS OF GROUPS

Galaxy	Group Affiliation	C21	C32	log (L_X^h/L_B) (ergs s^{-1} $L_{B,\odot}^{-1}$)	log (L_X^s/L_B) (ergs s^{-1} $L_{B,\odot}^{-1}$)
NGC 507	NGC 507 group	0.45	1.72	31.43	30.93
NGC 533	GH14	0.40	1.56	31.03	30.64
NGC 1399.....	Fornax Cluster	0.36	2.00	30.75	30.33
NGC 4472.....	Virgo South	0.65	1.56	30.55	29.99
NGC 5044.....	NGC 5044 group	0.47	1.50	31.92	31.48
IC 4329	IC 4329 group	0.39	1.51	30.91	30.40

obtain $L_X^h \propto L_B^{2.48\pm0.19}$, with a dispersion of 0.49 dex. Although this relation is flatter than the relation derived using all of the galaxies, it is still somewhat steeper than the value derived by White & Davis (1997), once they removed the cooling flow galaxies NGC 4486, NGC 4696, and NGC 1399 from their sample. The best-fit relations with and without the six group center galaxies are shown in Figure 1. It should be noted that there are other galaxies in our sample that lie at the center of groups (e.g., NGC 2300, NGC 3607, NGC 5846), but these groups are generally poor, and the integrated X-ray colors appear normal.

In Figure 2, the soft-band X-ray luminosity, L_X^s, is plotted versus the blue optical luminosity, L_B. The unweighted best-fit relation is $L_X^s \propto L_B^{1.94\pm0.17}$ with a dispersion of 0.45 dex. After excluding the six group center galaxies discussed above, we obtained a best-fit relation of $L_X^s \propto L_B^{1.75\pm0.16}$ with a dispersion of 0.39 dex. In the soft band, the X-ray–optical correlation is much flatter than for the hard band. The best-fit relations with and without the group center galaxies are shown in Figure 2.

Figure 3 shows the soft-band X-ray–to–optical ratio, log (L_X^s/L_B), versus the hard-band ratio, log (L_X^h/L_B). There is a tight, linear relation between log (L_X^s/L_B) and log (L_X^h/L_B) for galaxies with log $(L_X^h/L_B) > 30.4$ (group 4). However, for fainter X-ray galaxies in the range $29.7 < \log (L_X^h/L_B) < 30.4$, the slope flattens significantly; these galaxies all have log $(L_X^s/L_B) \approx 29.8$. (The few galaxies in this region of the plot that exhibit a lower value of L_X^s/L_B all have Galactic column densities that are near the upper limit for our sample, so it is possible that their soft X-ray emission is underestimated because of absorption. At any rate, the upper error bars on these galaxies are consistent with the L_X^s/L_B values for the rest of the groups 2 and 3 galaxies.) Finally, the X-ray faintest galaxies with log $(L_X^h/L_B) < 29.7$ (group 1) again show a crudely linear relation between L_X^s/L_B and L_X^h/L_B.

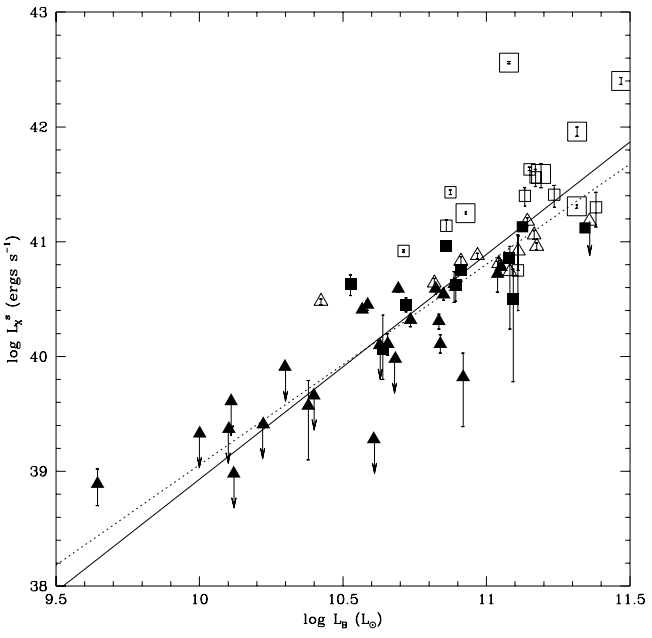

FIG. 2.—Logarithm of the soft-band (0.11–0.41 keV) X-ray luminosity, L_X^s, vs. the logarithm of the blue optical luminosity, L_B, for all of the galaxies in the sample. The notation is identical to that in Fig. 1. The best-fit power-law relations are $L_X^s \propto L_B^{1.94\pm0.17}$ (*solid line*) (whole sample) and $L_X^s \propto L_B^{1.75\pm0.16}$ (*dotted line*) (group center galaxies excluded from sample).

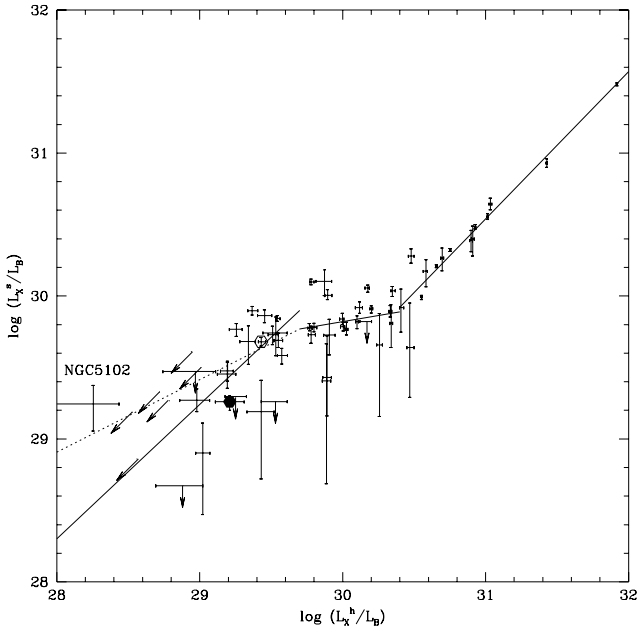

FIG. 3.—Logarithm of the soft-band X-ray–to–optical ratio, log (L_X^s/L_B), vs. the logarithm of the hard-band ratio, log (L_X^h/L_B), for all 61 galaxies in our survey. The solid lines show the best-fit linear relations for group 1, groups 2 and 3, and group 4 galaxies. In the case of group 1 galaxies, NGC 5102 was excluded from this fit. The dotted line is the best-fit relation for group 1 galaxies if NGC 5102 is included. Symbols with one-sided vertical arrows were detected in the hard band only, and symbols with one-sided slanted arrows were not detected in either band. The bulges of M31 and NGC 1291 are shown as a filled and open hexagon, respectively.

To quantify these trends, we derived the best-fit slope between log (L_X^s/L_B) and log (L_X^h/L_B) for the group 4, groups 2 and 3, and group 1 galaxies for which emission was detected in both bands. Galaxies with upper limits were excluded in the fit, although all of the galaxies were consistent with the trends found above. For group 4 galaxies, we find $L_X^s/L_B \propto (L_X^h/L_B)^{1.03\pm0.09}$. For groups 2 and 3 galaxies, we find $L_X^s/L_B \propto (L_X^h/L_B)^{0.18\pm0.22}$. Finally, for group 1 galaxies, we find $L_X^s/L_B \propto (L_X^h/L_B)^{0.50\pm0.19}$. This relation becomes nearly linear if NGC 5102 is excluded: $L_X^s/L_B \propto (L_X^h/L_B)^{0.94\pm0.32}$. This steeper relation for the group 1 galaxies is more consistent with the upper limits for galaxies that were undetected. Inspection of the 0.11–0.41 keV image of NGC 5102 shows a considerable number of foreground/background sources near the position of NGC 5102, so it is not clear if the source at the position of NGC 5102 is actually emission from the galaxy or just a positional coincidence with an unrelated source. The best-fit relations for group 1 (both with and without NGC 5102), for groups 2 and 3, and for group 4 are shown in Figure 3.

5. INTEGRATED X-RAY COLORS

In order to compare the average spectral properties of the galaxies in our sample, the integrated colors representing emission from the whole galaxy were determined for each galaxy in which X-ray emission was detected in all three bands. The size of the extraction region was chosen to be that radius that provided the highest signal-to-noise ratio in C21. Although this meant discarding all counts in bands 2

and 3 outside of this radius (which sometimes amounted to a large fraction of the total emission in the two harder bands), it was necessary to ensure that the colors C21 and C32 represented the emission from the same physical space within the galaxy. In addition, the extraction radius was always set to at least 1′ to reduce the effects of the energy-dependent point-spread function (PSF) of the PSPC on the colors. After the raw colors were determined for each galaxy, they were corrected for Galactic absorption according to the procedure outlined in § 3.

A plot of C21 versus C32 is shown in Figure 4 for all galaxies in the survey with detectable emission in all bands, along with the 1 σ error bars. The values for the integrated colors are also given in the last two columns of Table 2. It is obvious from Figure 4 that the X-ray faintest group 1 galaxies (*filled triangles*) are separated from the X-ray brightest group 4 (*open squares*). All group 1 galaxies with the exception of NGC 1427 at (C21, C32) = (0.19, 2.36) have C21 colors less than 0.3 and C32 colors consistent with 0.5–1.0. In contrast, the group 4 galaxies have C21 colors greater than 0.3 and C32 colors above 0.8. Group 2 (*filled squares*) and group 3 (*open triangles*) galaxies provide for a smooth transition in colors between the group 1 and 4 galaxies. The fact that X-ray–faint galaxies have relatively more very soft X-ray emission (lower C21) than X-ray–bright galaxies was hinted at by Kim et al.'s (1992) *Einstein* study, although their statistics were too poor to prove this for each galaxy individually. Pointed observations by *ROSAT* showed this to be true for a few of the faint X-ray galaxies with the highest fluxes (e.g., Fabbiano, Kim, & Trinchieri 1994; Pellegrini 1994). This study shows that all X-ray–faint early-type galaxies with detectable emission have excess very soft emission.

It is useful to compare the colors derived from the data to the colors predicted from various single-component thermal models once the models have been folded through the spectral response of the PSPC. Since the true X-ray emission mechanism of early-type galaxies over the entire X-ray spectrum is more complicated than a simple one-component model, these comparison models are intended only as a general description of the emission in the 0.1–2 keV energy range. At higher energies, stellar emission quite possibly contributes significantly to the X-ray emission. We present the colors for single-component thermal models because more complex spectral models with more than two free parameters are difficult to represent in a two-dimensional plot with data points. The colors expected from Raymond-Smith thermal models are shown as solid lines in Figure 5, which shows the same integrated color data for the galaxies as in Figure 4. Each track represents a different metallicity, and each point along a given track represents a different temperature. The X-ray–bright group 3 and group 4 galaxies lie in the same region of C21-C32 space as thermal models with temperatures between 0.6 and 1.5 keV and abundances between 20% and 100% of solar. This agrees with previous analyses of the X-ray spectra of the brighter galaxies (e.g., Buote & Canizares 1994, and the references in § 1). It is worth mentioning that abundance and temperature gradients may affect the conclusions drawn from single-component spectral models. The integrated colors represent the average emission properties of the galaxies, and the effect of gradients will be discussed in § 6.

It is possible that some of the galaxies in the sample harbor active galactic nuclei (AGNs) despite the fact that they are not listed in the Veron-Cetty & Veron (1996) catalog. However, if AGN emission were important in these galaxies, their X-ray colors would most likely be significantly different than galaxies without AGNs. The lack of

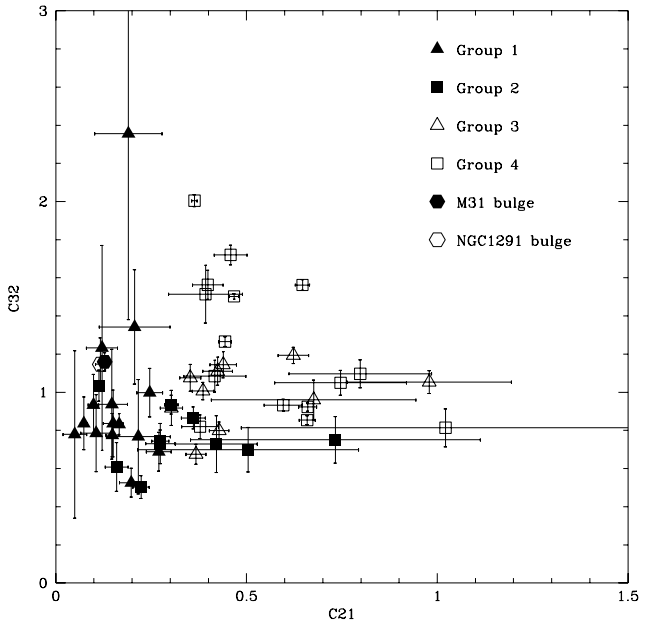

FIG. 4.—Integrated C21 and C32 colors for the 50 galaxies that had emission in all three bands, with the 1 σ errors. The filled hexagon represents the bulge of M31, and the open hexagon represents the bulge of NGC 1291.

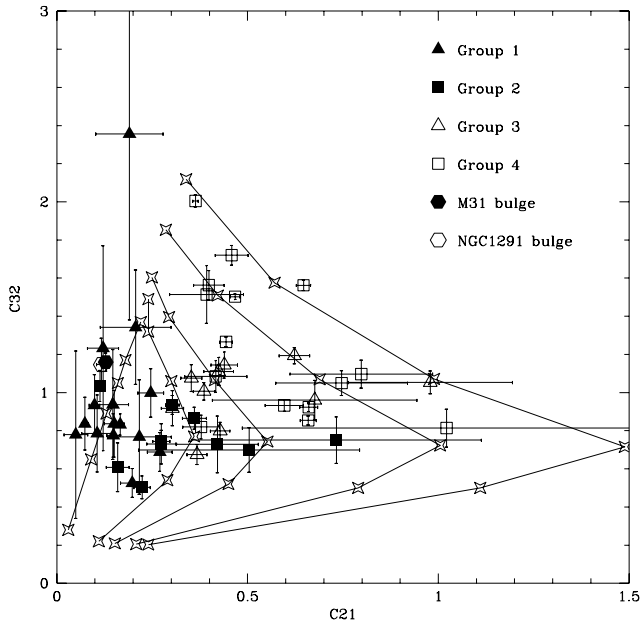

FIG. 5.—C21 and C32 colors from Fig. 4 shown with lines indicating the loci for simple thermal models for the emission. The solid lines represent the colors predicted from a variety of Raymond-Smith models, with each track representing a different metallicity: zero abundance, 10%, 20%, 50%, and 100% (*left to right*) of solar. Along a given track, each symbol represents a different temperature: 0.2, 0.4, 0.6, 0.8, 1.0, 1.5 keV (*bottom to top*).

conspicuous outliers on the color-color diagram suggests that it is unlikely that any galaxies with strong AGN X-ray emission remain in the sample.

A subgroup of the group 4 galaxies have lower C21 and higher C32 colors than the rest of the group 4 galaxies, which is indicative of higher temperatures as shown by the model tracks. As noted in § 4, these higher temperature group 4 galaxies all sit at the center of a group of galaxies. These galaxies are identified in Table 4. It seems likely that a deeper potential well due to the group is responsible for the higher temperatures and different colors than the rest of the group 4 galaxies.

Most of the X-ray faintest group 1 galaxies have colors that are consistent with very low abundance ($<20\%$ solar) thermal models with a variety of temperatures. A few of the group 1 galaxies have colors that are inconsistent with even zero metallicity and single-temperature optically thin thermal emission. The plausibility of low-metallicity gas being the source of the X-ray emission in these X-ray–faint galaxies will be discussed below (§ 7.3).

Davis & White (1996) find that absorption due to material that is intrinsic to the galaxy is not substantial in their sample of 30 galaxies. We have examined this possibility for our sample. We computed the colors of the same thermal models shown in Figure 5 but added a foreground absorbing screen with a column density of 10^{20} cm^{-2}. The absorbed model colors are shown as solid lines in Figure 6. By comparing to Figure 5, we see that C32 is hardly changed by the addition of the absorption component, but C21 is shifted significantly to the right. None of the galaxies in our sample fall within the region of C21-C32 space occupied by the absorbed models with abundances greater than 20% of solar. Therefore, we conclude that foreground column densities intrinsic to the galaxies $\gtrsim 10^{20}$ cm^{-2} are not present, unless the abundance in these galaxies is very low, and then only in the brightest X-ray galaxies. This comparison also serves as an indication that our procedure for correcting the observed colors for absorption is reasonably accurate.

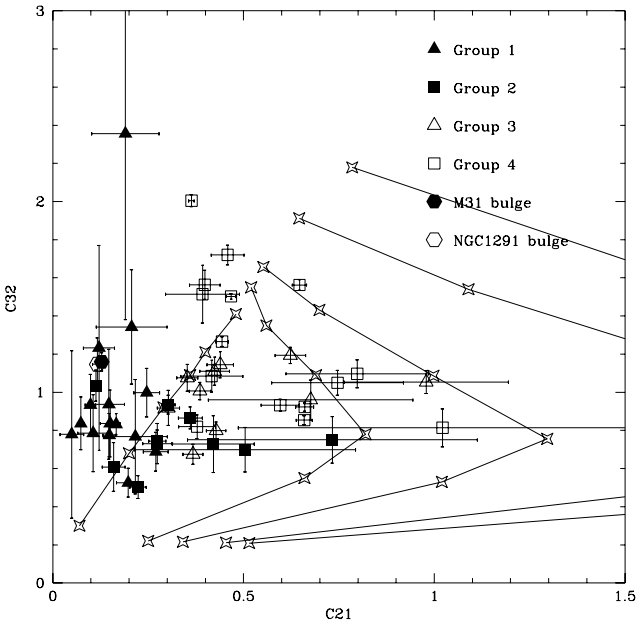

FIG. 6.—Same as Fig. 4, except the model thermal spectra have an extra foreground absorbing column density of 10^{20} cm^{-2}. The addition of the extra absorption shifts C21 to larger values (*to the right*) but hardly affects C32.

6. RADIAL COLOR VARIATION

In addition to the integrated colors, we also calculate the colors as a function of radius, C21(r) and C32(r), for each galaxy with enough counts to do so. In order to extract the maximum amount of spatial information consistent with the PSF of the PSPC and with reasonable statistical accuracy, we followed the following procedure. Counts were accumulated in annuli with widths of 30″, starting with an innermost circle with this radius. Succeeding annuli were combined until the colors from the combined ring could be determined with a signal-to-noise ratio of at least 4. When this occurred, we stopped accumulating counts in that ring and started another. Again, we combined 30″ annuli until this next ring had a signal-to-noise ratio of at least 4, and so on. This was repeated out to the last radial bin in which the signal-to-noise ratio was greater than 2. This was done to avoid creating radial bins that might be dominated by systematic errors in the background subtraction or vignetting correction, rather than the statistical errors. Note that the last bin does not necessarily satisfy the 25% accuracy criterion for the colors. We required that each ring be at least 1′ in radius or width in order to reduce the effects of the energy-dependent PSF of the PSPC.

The radial color profiles are presented in Figure 7 for all galaxies for which at least two spatial bins were obtained for C32. As was the case with the integrated colors, the radial color profiles also are distinctly different between different groups. Although all of the galaxies show a general decreasing radial trend in C21, the behavior of the C32 radial profiles is a function of the X-ray–to–optical luminosities. The X-ray brightest group 4 galaxies in general show an increase in C32 out to a few effective radii, before leveling off or decreasing somewhat at large radii. Group 3 galaxies show the same trend, although some galaxies in this group have a flat radial C32 profile. Group 2 galaxies show a flat or somewhat decreasing radial C32 profile. Finally, the few X-ray faintest group 1 galaxies for which a profile could be determined had a constant or somewhat decreasing C32 profile and a roughly constant C21 profile.

Figure 8 shows the radial color profiles of two selected galaxies on the C21-C32 diagram. The colors from a given galaxy are connected by solid lines, with arrows indicating the direction of increasing radius. We have chosen NGC 4649 as a suitable object to represent the higher X-ray luminosity galaxies of groups 3 and 4. As the galactocentric distance increases, the color change is nearly consistent with a track of constant metallicity and increasing gas temperature. Such a radial temperature variation has been found previously from detailed spectral fits to *ROSAT* PSPC data on X-ray–bright galaxies such as NGC 4636 (Trinchieri et al. 1994), NGC 4472 (Forman et al. 1993), and NGC 507 (Kim & Fabbiano 1995). This drop in temperature at the center of the galaxy can be interpreted as evidence for a cooling flow in these galaxies. To the extent that the color tracks differ from those for a constant abundance, they suggest that in general the iron abundance in the gas decreases with radius. Again, a similar trend has been found from detailed *ASCA* X-ray spectra for the more luminous X-ray galaxies (Mushotzky et al. 1994). Other galaxies in these groups show color variations that are consistent with an initial increase in temperature with increasing

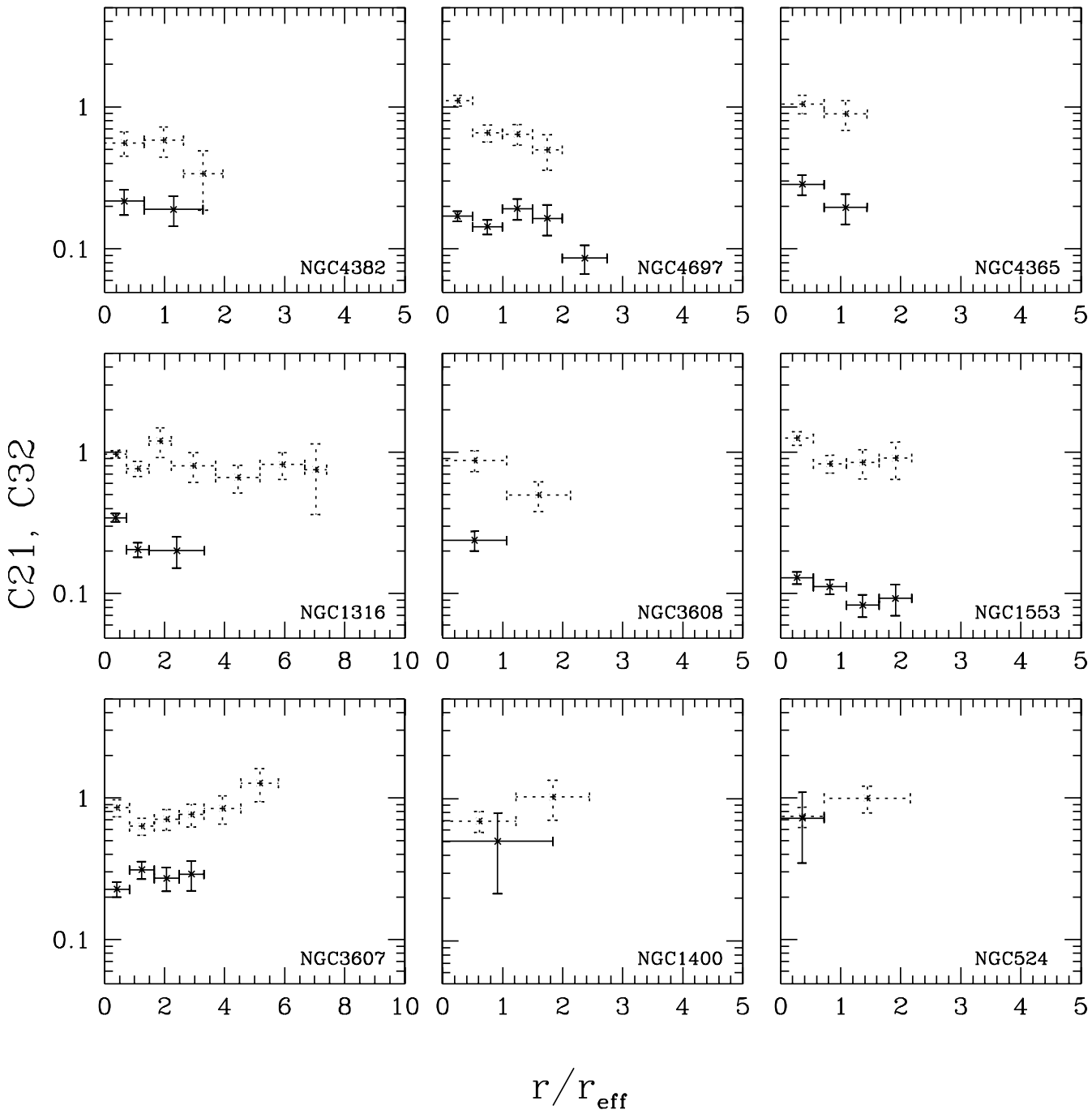

FIG. 7.—Radial profiles of the C21 (*solid lines*) and C32 (*dotted lines*) X-ray colors for galaxies with at least two spatial C32 bins. The colors are plotted vs. the projected radius in units of the optical effective radius. The galaxies are ordered by increasing L_X^h/L_B.

radius at small radii; at larger radii, the X-ray colors remain constant within the errors. These color profiles suggest that cooling is very significant in the central regions but that the gas is isothermal in the outer regions.

The situation is quite different for the few group 1 galaxies that have enough counts to determine the colors as a function of radius, as shown by the color profile of NGC 4697 in Figure 8. In this galaxy, the X-ray colors do not vary in the way expected for increasing gas temperatures with increasing radii. On the contrary, if the color variation were interpreted in terms of a single-temperature thermal model, one would require that the gas temperature decrease and iron abundance increase with radius. Moreover, many of the colors are inconsistent with any single thermal model, including an iron abundance of zero. The problems raised by the colors and color variations of group 1 galaxies are discussed further in § 7.3.

7. THE ORIGIN OF THE X-RAY EMISSION IN EARLY-TYPE GALAXIES

The C21-C32 plot (Fig. 4) and the log (L_X^s/L_B) versus log (L_X^h/L_B) relation (Fig. 3) both suggest that the X-ray emission in elliptical and S0 galaxies is complex and not the result of one mechanism. Here, we attempt to understand the diversity in X-ray spectral properties among galaxies with varying X-ray–to–optical luminosities.

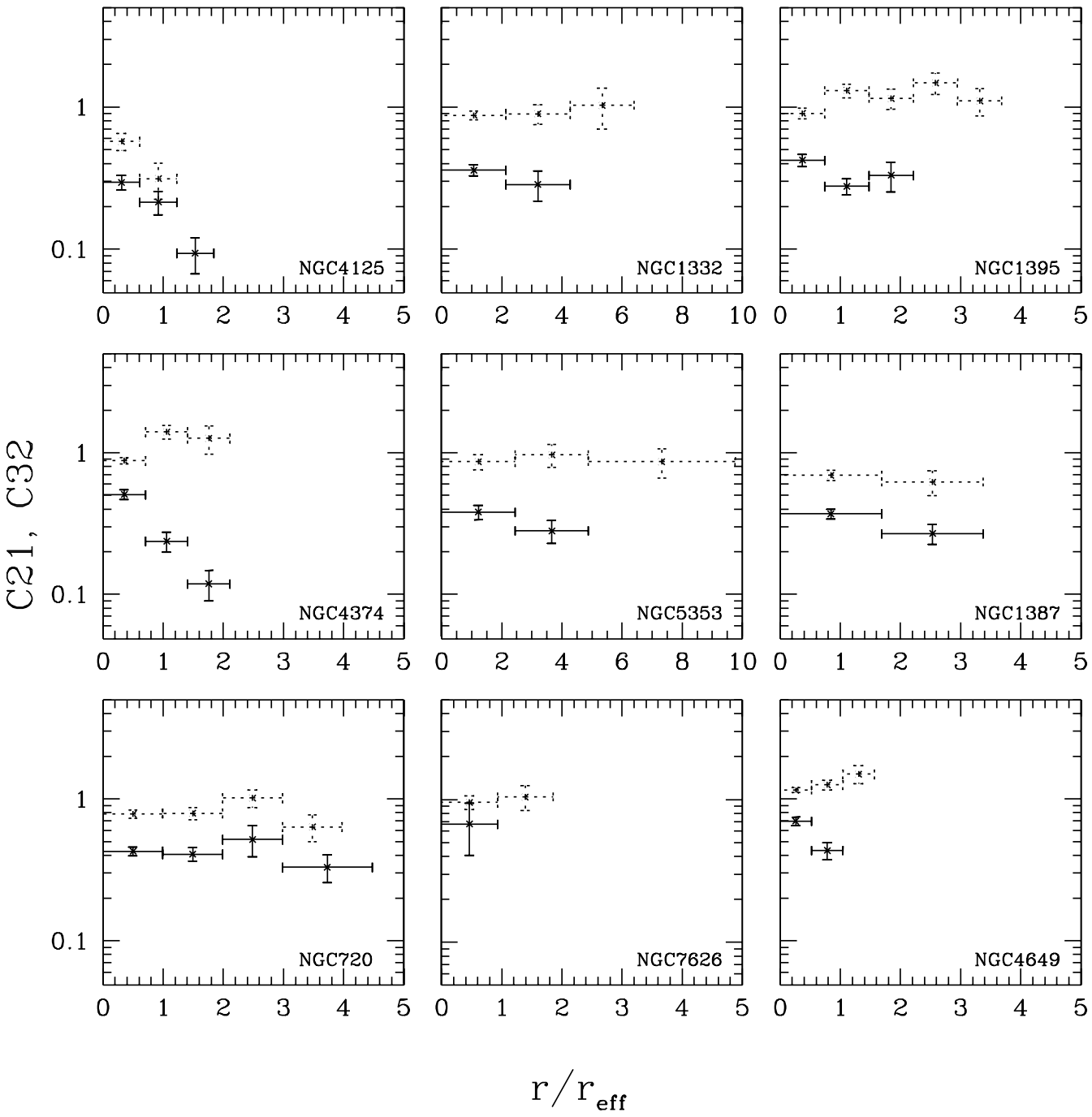

FIG. 7.—*Continued*

7.1. *Group 4 Galaxies*

Given their high X-ray luminosities and the fact that the nearest giant elliptical galaxies are all at the approximate distance of the Virgo Cluster, group 4 includes the galaxies with the highest observed X-ray fluxes. As a result, these galaxies have been studied in the most detail in the past. In particular, the brightest group 4 galaxies have high signal-to-noise spectra from *ROSAT* or *ASCA* which can be analyzed in detail. Not surprisingly, our integrated colors and color profiles are consistent with the results of these spectral studies. The X-ray emission of the group 4 galaxies is apparently predominantly thermal X-ray emission from hot gas with temperatures of 0.6–1.5 keV and metallicities $\sim 50\%$ of solar. The tight linear correlation found between $\log (L_X^s/L_B)$ and $\log (L_X^h/L_B)$ (Fig. 3) also suggests that a single emission mechanism, thermal emission by diffuse gas, is predominant in these galaxies.

In a survey of early-type galaxies observed with *ASCA*, Matsumoto et al. (1997) found a hard (5–10 keV), presumably stellar component in addition to a softer ISM component in nearly all of the galaxies observed. However, the 0.5–4.5 keV luminosity of this hard component was an order of magnitude less than that of the soft ISM component in the X-ray brightest galaxies. After adopting an average hard–to–soft component normalization from the Matsumoto et al. (1997) sample, this hard component was

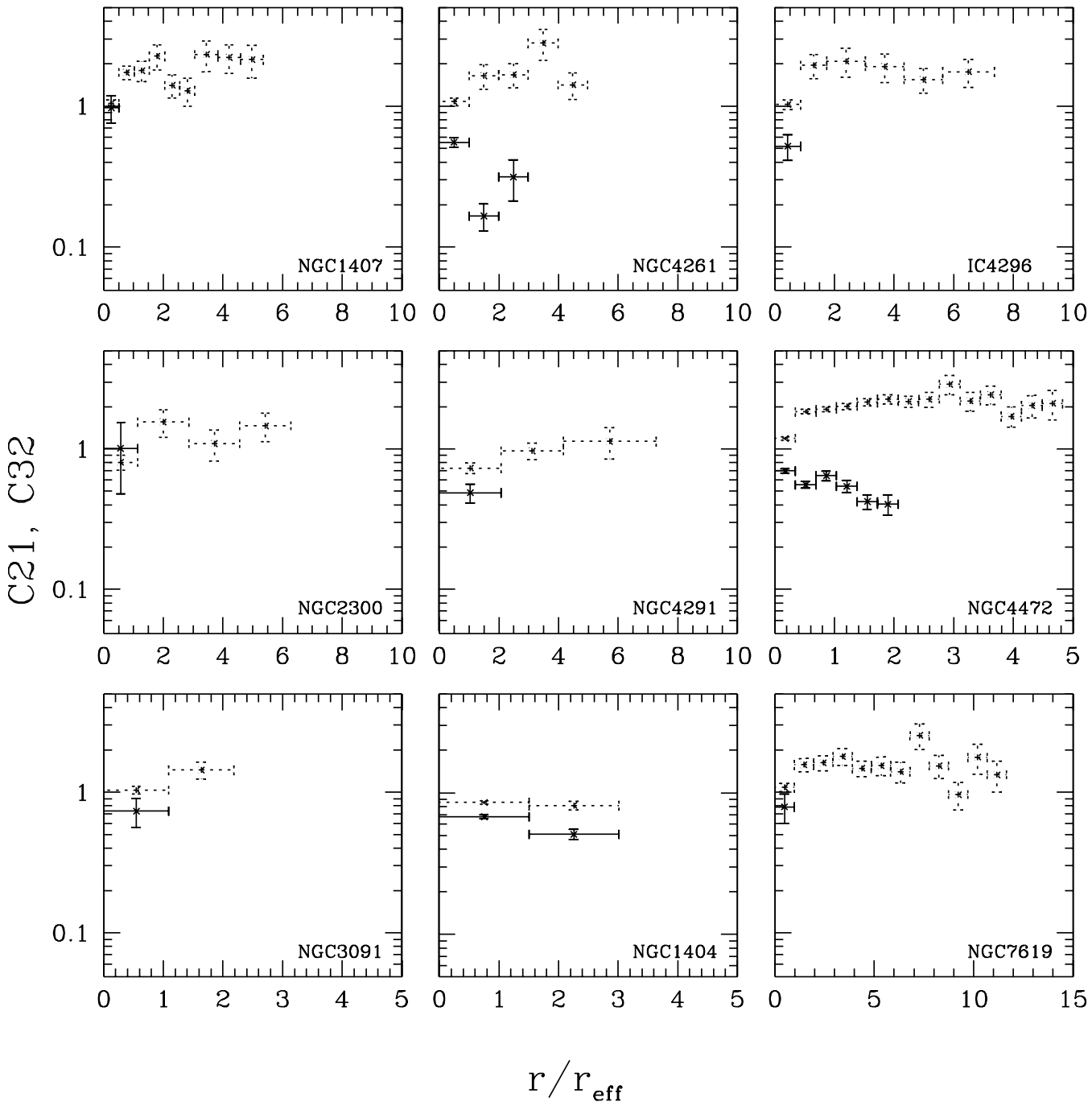

FIG. 7.—*Continued*

added to the models. The addition of the hard component to the existing models changed the model colors by no more than 15% for spectral models with temperatures 0.6 keV and greater. For models with temperatures below 0.6 keV, the colors were affected somewhat more, but not to the level where they became consistent with the observed colors.

In general, the color profiles indicate that the temperature of the gas increases with increasing galactocentric radius, which suggests that a cooling flow is present in most of these high-L_X/L_B systems.

The tight linear correlation found between log (L_X^s/L_B) and log (L_X^h/L_B) (Fig. 3) and the nonlinear increase of the X-ray luminosity in both bands with the optical luminosity implies that any stellar X-ray emission is completely swamped by the gaseous emission in the *ROSAT* band.

Many of the most luminous X-ray galaxies in group 4 are located at the centers of groups (Table 4). The higher X-ray luminosities of these galaxies may reflect gas that was trapped in the gravitational potential of the groups, with the brighter X-ray galaxies sitting in the deeper potential wells. Similarly, the harder X-ray colors of these galaxies may reflect the deeper potential well of the group.

7.2. *Group 2 and Group 3 Galaxies*

Below log $(L_X^h/L_B) = 30.4$, the log (L_X^s/L_B) versus log (L_X^h/L_B) relation flattens considerably (Fig. 3). One explana-

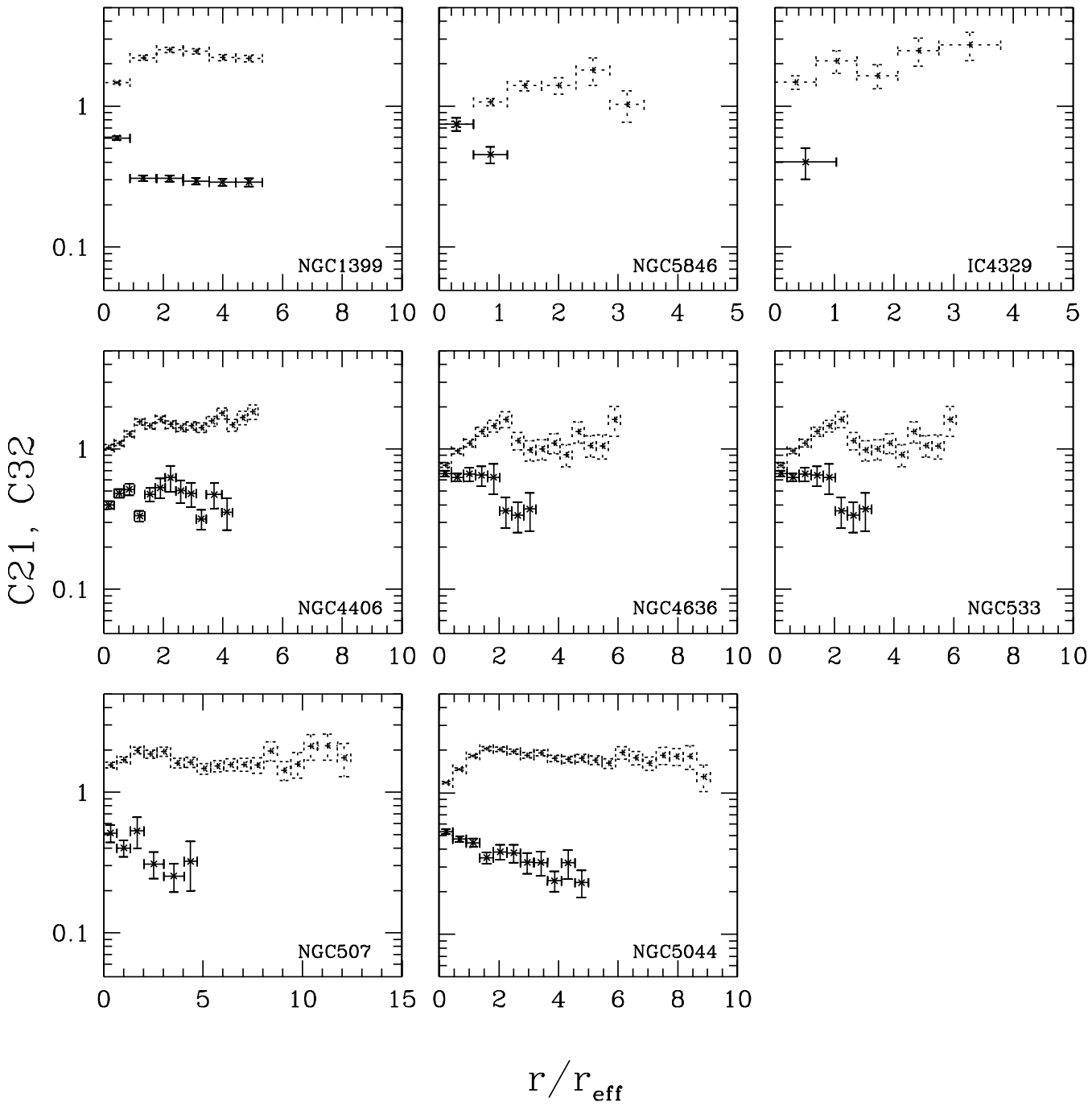

FIG. 7.—*Continued*

tion of this leveling off of L_X^s/L_B would be that the emission in the soft X-ray band in these galaxies is stellar in nature and thus directly proportional to the optical luminosity. However, this would not explain why L_X^s/L_B continues to decrease again once log (L_X^h/L_B) drops below 29.7. In addition, analyses of *ROSAT* and *ASCA* X-ray spectra of a few of these galaxies (e.g., Davis & White 1996; Matsumoto et al. 1997) show that the bulk of the emission is thermal emission from hot gas and subsolar abundances, much like group 4 galaxies. Unless the integrated stellar emission from these galaxies mimics the spectrum from hot gas, it is unlikely that we are seeing the stellar X-ray emission that must underlie the X-ray emission in all early-type galaxies at some level. Furthermore, the L_X^h/L_B value expected from a stellar component, derived from the Matsumoto et al. (1997) sample (see § 7.3 below), is 29.4, which is an order of magnitude less than where the flattening begins. Although stellar emission may become significant in the faintest group 2 galaxies ($L_X^h/L_B \sim 29.7$), it is unlikely that stellar emission is important for the brighter groups 2 and 3 galaxies.

The C21-C32 diagram (Fig. 4) provides an alternative explanation for this flattening. As L_X^h/L_B decreases, C21 decreases while C32 remains roughly constant. As the thermal emission models of Figure 5 show, this effect could be the result of variations in the abundance. To test this, we

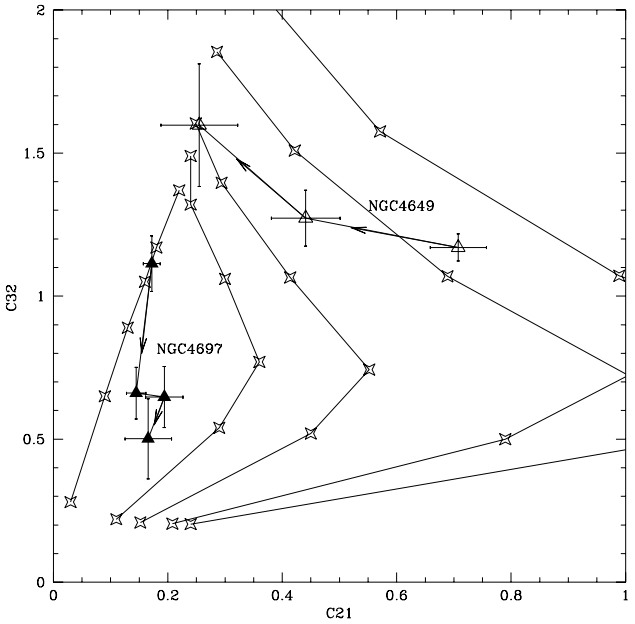

FIG. 8.—Spatial variation of the X-ray colors of two example galaxies are shown in the C21-C32 plane. The data points give the colors, while the arrows connecting them show the direction of increasing radius. The galaxies are labeled. NGC 4649 is an X-ray–bright, group 3 galaxy, while NGC 4697 is an X-ray–faint, group 1 galaxy. The model tracks are the same as in Fig. 5.

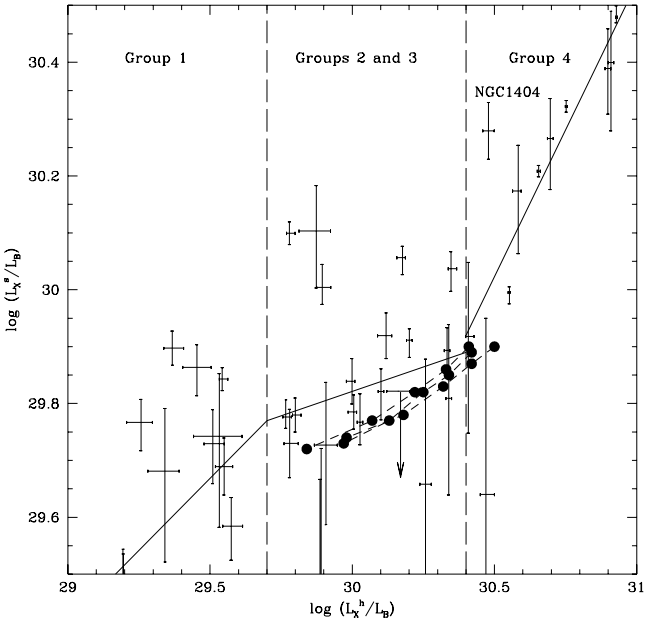

FIG. 9.—Enlarged view of the center of Fig. 3. The data point corresponding to NGC 1404 is indicated. The three dashed lines show the predicted log (L_X^s/L_B) and log (L_X^h/L_B) values for Raymond-Smith models with temperatures of 0.8, 0.4, and 0.6 keV (*top to bottom*) and abundances that vary along each curve from 10% of solar (*left*) to 50% of solar (*right*). The models assume a constant ratio of the volume emission measure of the gas to the optical luminosity.

have computed the luminosity expected in both the soft and hard X-ray bands for a series of one-component Raymond-Smith models with a constant emission measure but a variety of temperatures and metallicities. The X-ray luminosities were divided by a constant arbitrary blue luminosity, which yielded log (L_X^s/L_B) and log (L_X^h/L_B) values that best matched the average values of the groups 2 and 3 galaxies. The results are shown in Figure 9 for models with temperature of 0.4, 0.6, and 0.8 keV and abundances that ranged from 10% to 50% of solar. The three temperature tracks are shown as dashed lines.

We find that the hard–to–soft X-ray luminosity ratio varies little with temperature between 0.4 and 0.8 keV, with differences in this ratio being driven by abundance differences. As the abundance decreases, the hard X-ray luminosity decreases significantly faster than the soft X-ray luminosity for a given emission measure. The reason for this is apparently that the decrease in abundance reduces the strength of the iron *L*-line complex around 1 keV that dominates the hard-band emission at these temperatures. On the other hand, the soft band contains a larger fraction of continuum emission and is less affected.

This is just the trend seen for the hard and soft X-ray luminosities in groups 2 and 3 galaxies as L_X^h/L_B decreases. Furthermore, the change in log (L_X^h/L_B) in going from 50% solar to 10% solar abundance is 0.6 dex, nearly the same range over which L_X^h/L_B is seen to decrease for groups 2 and 3 galaxies. Thus, a variation in abundance for temperatures in the 0.4–0.8 keV range provides a simple, plausible explanation for why L_X^s/L_B decreases much more slowly than L_X^h/L_B.

We have searched the literature for all elliptical and S0 galaxies in our survey that have been observed by *ASCA* and for which abundances have been determined. The abundances for these galaxies are plotted in Figure 10 versus log (L_X^h/L_B). Unfortunately, only five groups 2 and 3 galaxies have published *ASCA* abundances, and the 90% errors are rather large, so we can draw no firm conclusion on the dependence of abundance on L_X^h/L_B for galaxies in these two groups until more groups 2 and 3 spectra have been analyzed. This figure does suggest that the abundance

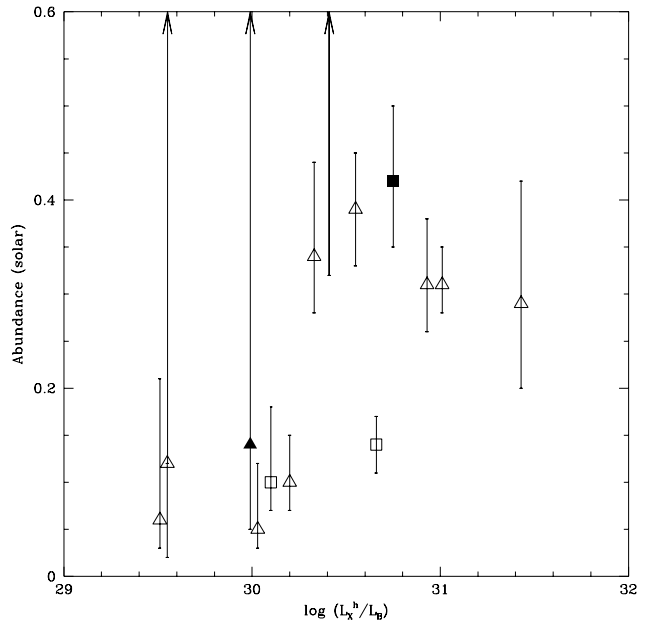

FIG. 10.—Abundances for galaxies in our sample as determined by *ASCA* as a function of log (L_X^h/L_B) with 90% error bars. Open triangles denote values from Matsumoto et al. (1997), open squares denote values from Loewenstein (1996), filled triangles denote values from Buote & Canizares (1997), and filled squares denote values from Arimoto et al. (1997).

does increase with L_X^h/L_B for galaxies with intermediate X-ray luminosities and that the abundances for group 4 galaxies are roughly constant, with the exception of NGC 1404. Group 4 galaxies do not exhibit the same flattening seen in groups 2 and 3 galaxies, apparently due to the fact that group 4 galaxies all have nearly the same abundance; they have higher L_X^h/L_B values than the groups 2 and 3 galaxies primarily because they sit at the center of groups of galaxies, not because of an abundance effect. The group 4 galaxy NGC 1404 has an anomalously low abundance, which would have the effect of making it underluminous in L_X^h/L_B for its L_X^s/L_B, as is observed in Figure 9.

In constructing the model curves in Figure 9, one important assumption we have made is that the volume emission measure of the hot gas is proportional to the stellar luminosity for the groups 2 and 3 galaxies. This would not be expected to be the case if the galaxies covered a large range in optical luminosity, because the radii and other properties of the galaxies would vary. However, the average blue luminosities for group 2 and group 3 galaxies are similar, $9.5 \pm 5.3 \times 10^{10}$ $L_{B,\odot}$ and $1.2 \pm 0.5 \times 10^{11}$ $L_{B,\odot}$, respectively. Furthermore, $L_X^h \propto L_B^{1.16\pm0.18}$ and $L_X^s \propto L_B^{0.86\pm0.19}$ for groups 2 and 3 combined. The nearly linear dependence of X-ray luminosity with optical luminosity is consistent with the assumption that the gas emission measure per unit stellar luminosity mass is constant for these galaxies. This is manifestly not true of the group 4 galaxies, although this may be due in part to group gas.

Finally, there are five groups 2 and 3 galaxies with significantly higher soft X-ray luminosities than predicted by this model. Two of these galaxies may really be group 4 galaxies that have been "misplaced" into group 3 because of an abnormally low abundance. As was seen with NGC 1404, a low abundance has the effect of shifting a galaxy to the left of the best-fit line in Figure 10. These two galaxies might have been shifted out of the group 4 domain because of their low abundance. It is unlikely that abundance effects can be responsible for the three anomalous group 2 galaxies, though. In these galaxies, the origin of the excess soft X-ray emission is unknown.

7.3. *Group 1 Galaxies*

As mentioned in § 5 above, group 1 galaxies have very soft C21 colors, unlike their X-ray–bright counterparts. The mean color values and standard deviations are $\langle C21 \rangle = 0.16 \pm 0.06$ and $\langle C32 \rangle = 0.99 \pm 0.41$ (Table 3). We will use these values to test possible X-ray emission mechanisms in these galaxies.

From Figure 5, we see that the average colors of group 1 galaxies could result from emission from diffuse gas with a temperature of $\sim$0.6 keV and a metallicity below 10% of solar. However, there are at least three problems with such a single-component thermal model. First, it seems unlikely that gas with such a low metallicity could exist in an elliptical galaxy. Assuming typical stellar mass-loss rates, Fabbiano et al. (1994) find that 10^8 $M_\odot$ of primordial, metal-free gas would be polluted to 10% metal enrichment by stellar winds in about 10^7 yr. Second, Fabbiano et al. (1994) found that, although a single-component, low-abundance model could not be ruled out as a fit to the *ROSAT* spectrum of the X-ray–faint galaxy NGC 4382, the *ASCA* observation of this galaxy was not consistent with this model. Third, the C21-C32 plot shows a few group 1 galaxies that have colors that are even softer than those predicted by a thermal model with zero metallicity. Finally, if the abundance-temperature tracks shown in Figure 9 are extended to zero metallicity, the tracks are consistent with the luminosities of only the brightest of the group 1 galaxies [$\log (L_X^h/L_B) \gtrsim 29.3$]. Given the above arguments, we will abandon the single thermal component, low-abundance hypothesis.

Previous authors (Fabbiano et al. 1994; Pellegrini 1994; Kim et al. 1996) have found that a two-component model also provides an adequate fit to the spectra of low-L_X/L_B galaxies. In general, the two components that are required are a soft component, with $kT \sim 0.2$ keV and solar abundance, and a hard component with a temperature of $\sim$5 keV. The $\sim$5 keV model component is believed to be the integrated emission from a population of low-mass X-ray binaries (LMXBs), as is found in the bulges of spiral galaxies (Trinchieri & Fabbiano 1985). Matsumoto et al. (1997) detected the presence of such a hard component in many elliptical and S0 galaxies of varying L_X/L_B. They also found that the X-ray luminosity of this component scales linearly with the optical luminosity, which is consistent with a stellar origin. The X-ray colors predicted for the hard component are C21 = 0.30 and C32 = 1.72, if it is modeled as thermal bremsstrahlung at a temperature of 5 keV.

The origin of the soft X-ray component is less clear. It has been suggested that the soft component is from the integrated emission of M-star coronae, from RS CVn binary systems, from supersoft sources like those observed in our Galaxy, M31, and the Magellanic Clouds, or from diffuse interstellar gas at a temperature of 0.2–0.4 keV (Pellegrini & Fabbiano 1994).

The faintest elliptical galaxies are believed to have overall properties and stellar populations similar to the bulges of large spiral galaxies. The nearest bulges (e.g., M31) are close enough that individual X-ray sources can be resolved. Thus, it is useful to determine the X-ray colors and X-ray–to–optical luminosity ratios of nearby spiral bulges; this can provide a strong test of stellar models for the origin of the X-ray emission in faint elliptical galaxies.

M31 is the best candidate to study because of its proximity. To determine if M31 is similar to the group 1 early-type galaxies in its X-ray properties, we extracted the archival *ROSAT* PSPC data on images covering the center of the bulge of this galaxy. We determined the integrated X-ray fluxes of the bulge in our bands. In doing so, we did not exclude point sources within the bulge, since these sources cannot be resolved in more distant early-type galaxies. We have determined the L_X^s/L_B and L_X^h/L_B values for the inner 10′ of M31, which corresponds to one effective radius for the bulge (2 kpc at a distance of 690 kpc). We assumed an integrated blue magnitude of 5.39 within one effective radius (Walterbos & Kennicutt 1988). The total soft and hard luminosities within 1 $r_{\rm eff}$, assuming our standard spectral model used for the sample, were 9.54×10^{38} and 8.47×10^{38} ergs s^{-1}, respectively. This corresponds to $L_X^s/L_B = 29.26$ and $L_X^h/L_B = 29.21$, which places the bulge of M31 within the observed range of values for group 1 galaxies (Fig. 3).

We also determined the X-ray colors for the bulge of M31. For comparison to the point-source catalog of Supper et al. (1997), we derived the colors for the inner 5′ of the bulge. We obtained (C21, C32) = (0.13, 1.16), corrected for foreground absorption ($N_H = 6.73 \times 10^{20}$ cm^{-2}); although the absorption is above our cutoff limit, this should not

introduce substantial errors into the determination of the colors. Thus, the integrated X-ray colors for the inner bulge of M31 are consistent with the colors of the faintest X-ray galaxies (Fig. 4). In particular, the bulge of M31 has essentially the same very soft C21 color as in elliptical and S0 galaxies.

However, the bulk of the X-ray emission from the bulge of M31 has been resolved into a relatively small number of luminous, discrete X-ray sources. For example, Supper et al. (1997) detected 22 point sources within 5′ of the center of M31. They also find that these 22 sources comprise 75% of the total flux within 5′ of the center of M31. Thus, any emission from unresolved sources or a diffuse component is not a major contributor to the total X-ray emission within the bulge. Supper et al. (1997) tabulated the count rates in the same three X-ray bands we use to determine X-ray colors. Three of the sources were detected only in the soft band and are most likely supersoft sources. The rest of the sources are most likely LMXBs. By summing the count rates in the three bands for the 22 sources, we derived the X-ray colors for the sum of emission from the discrete sources and corrected them for foreground absorption. The colors obtained were (C21, C32) = (0.08, 1.15). Thus, the colors from the sum of discrete sources in the bulge of M31 are consistent both with the integrated X-ray colors of the bulge and with the colors of the faintest X-ray galaxies (Fig. 4). Since the discrete sources provide most of the X-ray flux from the bulge of M31, the first result is not terribly surprising. Apparently, the source of the remaining 25% of unresolved flux within the bulge does not affect the colors to a great extent. It might raise the C21 value somewhat; if so, the diffuse emission is harder than the discrete emission at low energies. Removing the three supersoft sources found in the bulge does not change the integrated X-ray colors appreciably.

The comparison between the X-ray colors of early-type galaxies and those of the discrete sources in M31 shows that the very soft component in elliptical and S0 galaxies can be explained simply as emission from luminous, discrete binary X-ray sources, which are probably mainly LMXBs. Apparently, this was not appreciated earlier because most previous studies assumed too simple a model for the average X-ray spectra of LMXBs in early-type galaxies. In particular, the colors obtained for the bulge sources of M31 (0.08, 1.15) are clearly at odds with the colors derived from a 5 keV bremsstrahlung model (0.30, 1.72), which has commonly been used to describe the hard emission from LMXBs.

This suggests that the X-ray spectra of LMXBs contain a soft component in addition to a $\sim$5 keV component. As a further test of this hypothesis, we have done a more detailed analysis of the integrated X-ray spectrum of the bulge of M31. From the archival data of M31, we extracted the full-resolution spectrum of the inner 5′ of the bulge. The energy channels were rebinned to contain at least 20 counts, and a background spectrum, extracted from an annulus of 30′–40′ and corrected for vignetting, was scaled to and subtracted from the source spectrum. The background-subtracted spectrum contained 3003 counts. The results of the modeling of the X-ray spectrum of the bulge of M31 are summarized in Table 5.

Previous spectral modeling of the bulge of M31 with *Einstein* data by Fabbiano, Trinchieri, & Van Speybroeck (1987) found that the spectrum from the inner 5′ of the bulge was fit well by a bremsstrahlung model with $kT = 13.5$ keV and an absorbing column density somewhat less than the Galactic value. Here, we fit the spectrum of the bulge of M31 with Raymond-Smith models. Since the bulk of the emission from M31 is due to discrete LMXBs, where the emission is not mainly from collisionally ionized, diffuse, optically thin plasma, we do not attach any real physical significance to the parameters of these fits. Rather, we use this model to better compare to the results of previous spectral fits to early-type galaxies, which employ the Raymond-Smith model (e.g., Fabbiano et al. 1994).

We first attempted to fit the spectrum with a one-component Raymond-Smith model with variable abundance and Galactic absorption. This yielded an adequate fit to the data ($\chi^2 = 123.0/100$ degrees of freedom). The best-fit temperature was 0.78 keV, and the best-fit abundance was zero. This model is very reminiscent of the model that adequately fit the *ROSAT* spectra of several X-ray–faint galaxies but not the *ASCA* spectra of NGC 4382 (Fabbiano et al. 1994; Kim et al. 1996). However, as was the case for the X-ray–faint galaxies, this is not a plausible model for the integrated emission from LMXBs because it lacks the very hard component seen in these objects individually and in the *ASCA* spectra of elliptical galaxies. The temperature derived for this model is significantly less than the value determined by *Einstein* using a bremsstrahlung model, although an absorbing column density less than the Galactic value was found to yield the best fit to the *Einstein* data (Fabbiano et al. 1987), whereas we have fixed the column density at the Galactic value.

Next, a two-component Raymond-Smith model with abundances fixed at solar was used to fit the spectra. The fit was unacceptable, with $\chi^2 = 163.7$ for 99 degrees of freedom. The best-fit parameters were $kT_1 = 0.19$ keV and $kT_2 = 3.75$ keV. This is remarkably similar to the values obtained from the spectra of X-ray–faint galaxies. However, unlike the X-ray–faint galaxies, the observation of M31 contained enough counts to rule out this model.

We find that a vast improvement is made in the fit if we allow the abundance of the soft component to vary. Doing so reduces χ^2 to 100.5 for 98 degrees of freedom. The soft-component temperature was found to be $kT_1 = 0.36$ keV

TABLE 5

SPECTRAL FITS TO THE BULGE OF M31

Model	N_H (cm^{-2})	kT_1 (keV)	Z_1 ($Z/Z_\odot$)	kT_2 (keV)	Z_2 ($Z/Z_\odot$)	χ^2	Degrees of Freedom
1.....	6.73×10^{20}	$0.78^{+0.07}_{-0.06}$	$0^{+0.004}_{-0.00}$	...	...	123.0	100
2.....	6.73×10^{20}	$0.19^{+0.01}_{-0.01}$	1.00 (fixed)	$3.75^{+2.16}_{-1.13}$	1.00 (fixed)	163.7	99
3.....	6.73×10^{20}	$0.36^{+0.09}_{-0.06}$	$0.012^{+0.012}_{-0.005}$	>6.4	1.00 (fixed)	100.5	98

NOTE.—All errors are 90% confidence limits for one interesting parameter.

(0.30–0.45 keV) with an abundance of less than 3% of solar, and the hard-component temperature was $kT_2 > 6.4$ keV (all errors are quoted at the 90% confidence level).

Due to the very low abundance of the soft component, we hesitate to attach a physical significance to this two-component model for the X-ray emission from LMXBs. Nonetheless, the observations do show that a soft component should be expected from the integrated emission from LMXBs in an old stellar population. One does not need to invoke a separate class of X-ray–emitting objects to account for the soft X-ray emission in X-ray–faint elliptical galaxies, especially for the faintest of the group 1 galaxies whose X-ray colors and L_X/L_B ratios are fully consistent with those of the bulge of M31. A definitive confirmation of this prediction will be possible after the launch of *AXAF*. The backside-illuminated CCD chips of the *AXAF* CCD imaging spectrometer (ACIS) instrument on-board *AXAF* will provide the needed soft energy response and spatial resolution to resolve LMXB X-ray emission for early-type galaxies at a distance of Virgo or closer. The brightest group 1 galaxies may contain an additional soft component, which we will discuss in § 8.4.

We have also calculated the X-ray colors of the bulge of the bright Sa galaxy NGC 1291 to verify the results found for M31. We have assumed an integrated blue magnitude of 10.73 within an effective radius of 48″ (3.2 kpc at a distance of 13.8 Mpc; de Vaucouleurs 1975) for this galaxy. After correcting for absorption (2.24×10^{20} cm^{-2}), we derive integrated colors of (C21, C32) = (0.12, 1.15). These values are virtually identical to those obtained for M31. We also found that $L_X^s/L_B = 29.68$ and $L_X^h/L_B = 29.43$ for the bulge of NGC 1291. These values are somewhat higher than those that were found for M31 but are still within the range of observed values for X-ray–faint galaxies. A spectral fit of the bulge of NGC 1291 was performed by Bregman, Hogg, & Roberts (1995). They found that a two-component Raymond-Smith model with abundances fixed at solar provided a good fit to the data and yielded temperature values of $kT_1 = 0.18$ and $kT_2 = 1.91$ keV. These values are consistent with the temperatures derived for the bulge of M31 using an identical spectral model (see model 2 in Table 5). Although this model did not provide an adequate fit to the spectra of M31, the observation of NGC 1291 contained only one-third the number of counts of the M31 observation, so it is not surprising that solar abundances could not be ruled out for the soft component of NGC 1291.

Obviously, such a soft component in the X-ray emission from LMXBs should be readily observable in Galactic LMXBs, if it were not for the fact that nearly all of the LMXBs in our Galaxy lie in directions of high hydrogen column densities because they are concentrated to the central regions of the Galactic bulge. Such a soft component would be completely absorbed in these cases. However, the LMXB Her X-1 is relatively nearby and in a direction of low Galactic column density (1.73×10^{20} cm^{-2}). Observations of Her X-1 with *ROSAT* (Mavromatakis 1993) and *ASCA* (Vrtilek et al. 1994; Choi et al. 1996) find that a soft component described by a blackbody model with $kT = 0.1$ keV or a bremsstrahlung model with $kT = 0.2$ keV is needed in addition to a power-law model (for the harder X-ray emission) in order to fit the spectrum. The X-ray colors derived from the archived *ROSAT* data were found to be (C21, C32) = (0.08, 1.56) for Her X-1. Thus, the soft component seen in X-ray–faint galaxies and the bulges of M31 and NGC 1291 also appears to be present in the spectrum of at least one LMXB in our Galaxy, as indicated by its low C21 value. Although the C32 value of Her X-1 is somewhat higher than that of the group 1 galaxies or the bulge of M31, it falls within the range of observed C32 values found for individual LMXBs in the bulge of M31.

If NGC 5102 is excluded, the best-fit relation between L_X^s/L_B and L_X^h/L_B is nearly linear (Fig. 3). Along with the fact that the X-ray colors of most of the group 1 galaxies are consistent with emission from stellar emission as shown above, this suggests that most group 1 galaxies share the same single X-ray emission mechanism, with some galaxies having more X-ray emission per unit blue luminosity than others. At first this may seem at odds with the results of Matsumoto et al. (1997), who analyzed *ASCA* spectra from a sample of elliptical and S0 galaxies and found that all of their galaxies but one had a very hard X-ray spectral component. This hard component was consistent with a temperature of about 5 keV and was attributed to the emission from LMXBs. The luminosity of this hard component scaled linearly with the blue luminosity of the galaxy. We took the ratio of the 0.5–4.5 keV X-ray luminosity per unit optical luminosity from their paper and converted the X-ray luminosity to our hard band (0.52–2.02 keV), assuming model 3 of the fit for the bulge of M31 (see Table 5). This model gave nearly the same conversion factor as a 5 keV thermal bremsstrahlung model, since the soft component of model 3 contributes very little emission in the 2.0–4.5 keV range. If one excludes galaxies in their sample that may harbor active nuclei, this leads to a *ROSAT* hard-band X-ray–to–optical ratio of $\log (L_X^h/L_B) \approx 29.4$. This might be a slight underestimate because of the fact that some of the 0.5–4.5 keV flux from the soft component of Matsumoto et al.'s (1997) spectral fits is also from LMXB emission and has not been included in the calculation. This value is consistent with the luminosity ratios for the more luminous of the group 1 galaxies and for the bulges of M31 and NGC 1291.

However, Figure 3 shows that there are five galaxies that have upper limits on L_X^h/L_B that are at least a factor of 3 less than the value derived from the Matsumoto et al. (1997) correlation. For example, NGC 5102 has an order of magnitude less hard X-ray emission than expected for its blue luminosity, if the hard component scales linearly with optical luminosity. The same is true for the nearby dwarf elliptical NGC 205, which was not included in our sample because it did not meet the requirements stated in § 2 but nonetheless had an upper limit on $\log (L_X^h/L_B)$ of 28.27, a factor of 10 less than expected.

One possible explanation for the discrepancy may be that the galaxies in our sample with upper limits on the L_X^h/L_B ratios significantly less than 29.4 have fewer LMXBs per unit blue luminosity than the rest of the galaxies in the sample. Since LMXBs contain accreting neutron stars, the number of LMXBs in a given galaxy would decrease if fewer massive stars have been formed in the galaxy. This would imply that fainter elliptical galaxies had a steeper initial mass function. In fact, this theory has been proposed to explain the trend of increasing Mg/Fe ratios in elliptical galaxies as a function of increasing mass (Worthey, Faber, & Gonzalez 1992). If Mg is produced primarily by Type II supernovae and Fe by Type Ia supernovae, higher Mg/Fe ratios for larger elliptical galaxies could imply a higher rate of Type II supernovae and of neutron star production. Models by Matteucci (1994) show that flattening the initial

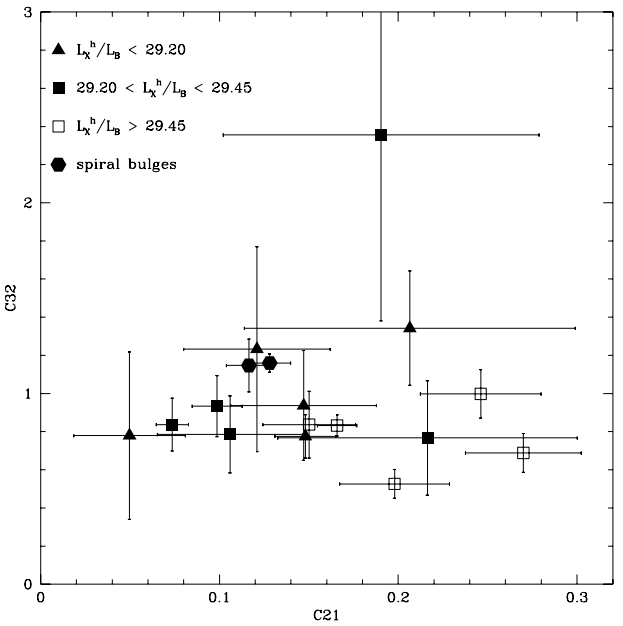

FIG. 11.—X-ray colors C21 and C32 are plotted against one another for the group 1 galaxies. These galaxies have been subdivided into three L_X^h/L_B classes; the symbols and corresponding luminosity ratio ranges are shown at the upper left. We have also plotted the colors of the two spiral bulges NGC 1291 (*left*) and M31 (*right*) as filled hexagons. The faintest X-ray galaxies have colors consistent with those of the two bulges (*hexagons*), but the five brightest group 1 galaxies (*open squares*) have distinctly different colors. These five galaxies are NGC 5866, NGC 4382, NGC 4697, NGC 4365, and NGC 1380.

mass function for more massive galaxies also predicts the $M/L_B \propto L_B^{0.2}$ relation that is seen in elliptical galaxies.

The five galaxies in the sample (plus NGC 205) with unusually low L_X^h/L_B values all have optical luminosities below $1.7 \times 10^{10}\ L_{B,\odot}$ and are considerably fainter (and presumably less massive) than the rest of the galaxies in the sample (see Fig. 1). On the other hand, the Matsumoto sample consisted mostly of luminous elliptical galaxies. According to the above argument, these galaxies should have fewer high-mass stars per unit blue luminosity available to make the neutron stars present in LMXBs. Matteucci (1994) argued that the slope of the initial mass function flattened from $x = 1.35$ (the Salpeter initial mass function) in fainter elliptical galaxies to $x = 0.95$ in brighter elliptical galaxies. This change will produce about 2.5 times fewer stars in the mass range 8–100 $M_\odot$ per optical luminosity in fainter elliptical galaxies as compared to brighter ones. We assume that only stars that are initially more massive than 8 $M_\odot$ evolve into neutron stars or black holes. This difference might be large enough to account for the lower proportion of LMXBs in most of the fainter group 1 galaxies, but not in NGC 5102 or NGC 205. It should be noted, though, that the optical luminosity of the bulge of M31 is rather low ($\sim 10^{10}\ L_{B,\odot}$), yet it has only a slightly lower than the expected log (L_X^h/L_B) value (29.21).

It is also possible that fluctuations in the small number of active LMXBs in faint early-type galaxies contribute to the variation in the X-ray–to–optical luminosity ratio. In particular, both NGC 5102 and NGC 205 have very low optical luminosities ($4.4 \times 10^9\ L_{B,\odot}$ for NGC 5102 and $2.0 \times 10^8\ L_{B,\odot}$ for NGC 205). If the average X-ray–to–optical luminosity ratio of faint elliptical galaxies is log (L_X/L_B) $\approx$ 29.4, then we would expect an X-ray luminosity of $L_X \approx 9 \times 10^{38}$ ergs s^{-1} for NGC 5102 and $L_X \approx 4 \times 10^{37}$ ergs s^{-1} for NGC 205. Particularly in the latter case, this would correspond to a small number of LMXBs.

Next we address the issue of why group 1 galaxies do not appear to have a significant ISM component as do their X-ray–bright counterparts. Detailed hydrodynamical simulations of the evolutionary behavior of the gas flow in elliptical galaxies by Loewenstein & Mathews (1987) show that bright, massive galaxies develop hot, gaseous halos after the Type II supernovae rate declines early in the galaxy's history. On the other hand, less massive galaxies are able to sustain a wind due to Type Ia supernovae. This wind drives the gas lost from stars out of the galaxy. The efficiency of wind mass loss depended on the assumed Type Ia supernovae rate and the presence and distribution of a dark matter halo. Later work by David, Forman, & Jones (1991) extended the simulations to include galaxies with luminosities as low as $10^9\ L_{B,\odot}$ and found basically the same results. The hydrodynamical models of Ciotti et al. (1991) suggested that hot gas in elliptical galaxies undergoes a three-stage (wind, outflow, inflow) evolution. All three studies concluded that galaxies covering the range of observed L_X/L_B values can be described in terms of differing hydrodynamical states of the gas ranging from supersonic winds to partial winds to cooling flows, depending on the galaxy's mass distribution and supernovae rate. Since the group 1 galaxies have the lowest optical luminosities and velocity dispersions in the sample, they should have shallower potential wells and could still be in the wind stage of their evolution.

If this argument is correct, then there should exist galaxies that have some but not all of their ISM removed. These galaxies would have comparable amounts of X-ray emission from the stellar and gaseous components. If so, these galaxies might have colors that differ somewhat from those of the purely stellar sources, such as the bulges of M31 and NGC 1291. To search for this, we have subdivided the 15 group 1 galaxies for which colors were determined into three groups based on L_X^h/L_B. The X-ray colors of these galaxies are shown in Figure 11. The two lowest L_X^h/L_B subgroups among group 1 galaxies (*filled triangles and filled squares*) have colors that scatter around those of the spiral bulges (*hexagons*), at least within the errors. On the other hand, the highest L_X^h/L_B subgroup (*open squares*) has colors that are distinctly different than those of the bulges. This could be explained by the presence of an additional soft component with C21 $\gtrsim$ 0.25 and C32 $\lesssim$ 0.7. This extra soft component would naturally explain why these galaxies have higher L_X/L_B values than the X-ray faintest galaxies. Below, we show that an ISM provides the most reasonable explanation for the additional soft component.

8. ALTERNATIVES FOR THE SOFT COMPONENT IN GROUP 1 GALAXIES

Previous authors (Kim et al. 1992; Pellegrini & Fabbiano 1994) have suggested that the integrated emission from M-star coronae, RS CVn binary stars, supersoft sources, or a warm ISM is responsible for the soft component found in group 1 galaxies, since these sources have the soft X-ray properties needed to explain the soft emission. However, the general consensus was that none of these mechanisms is entirely responsible for the soft X-ray emission. Earlier, we showed that LMXBs are probably responsible for the soft emission in the X-ray faintest galaxies, not the sources men-

tioned above. Here, we present further arguments as to why these sources cannot be substantial contributors to the X-ray emission in the X-ray faintest galaxies, although a warm ISM may be present in the brighter group 1 galaxies.

8.1. *M-Star Coronae*

Although intrinsically faint X-ray sources, M dwarf stars can be a source of substantial X-ray emission because of the sheer number of M stars relative to dwarf stars of earlier spectral types. M stars are also known to possess soft X-ray characteristics (Giampapa et al. 1996). However, it is unlikely that M dwarf stars are bright enough to produce the required X-ray luminosity. As pointed out by Pellegrini & Fabbiano (1994), if one assumes a Salpeter initial mass function and an appropriate mass-to-light ratio for elliptical galaxies, the average X-ray luminosity per M star must be 2×10^{28} ergs s^{-1} to account for the very soft X-ray emission in the X-ray–faint galaxy NGC 4365. Schmitt, Fleming, & Giampapa (1995) show that the average X-ray luminosity of stars in the solar neighborhood is $\sim 3 \times 10^{27}$ ergs s^{-1}. This is likely to be a significant overestimate of the average X-ray luminosity of M stars in old stellar systems, as the X-ray luminosity of stars is expected to decrease with age as the rotation of the star (and hence magnetic activity that produces the X-ray emission) decreases (Skumanich 1972).

Another test of the average X-ray luminosity of older M dwarf stars is provided by globular clusters. Given that globular clusters and elliptical galaxies possess similar stellar populations, X-ray emission from any stellar source should scale with optical luminosity between the two systems. To search for a diffuse X-ray component in globular clusters, we extracted the *ROSAT* PSPC observation of NGC 6752 from the archive. We selected this globular cluster because of its low Galactic column density ($N_{\rm H} = 2.40 \times 10^{20}$ cm^{-2}; Stark et al. 1992), its proximity (distance of 4.2 kpc), and its bright apparent blue magnitude, $m_B = 5.99$, which corresponds to a luminosity of $1.1 \times 10^5\ L_{B,\odot}$ (Peterson 1993). After cleaning, the exposure was 4939 s. The X-ray luminosity in the soft band was determined within the half-light radius of 115″ (Trager, Djorgovski, & King 1993), using the same spectral model as was used for the galaxy sample. A 1 σ upper limit of 9.48×10^{31} ergs s^{-1} was obtained for the 0.11–0.41 keV luminosity within the half-light radius, corresponding to an upper limit on $L_{\rm X}^s/L_B$ of 27.23. This is a factor of nearly 300 less than the $L_{\rm X}^s/L_B$ value of the X-ray–faint galaxies NGC 4365 and NGC 4382.

These limits on the diffuse X-ray emission from globular clusters also apply to any other stellar source for the soft X-ray emission in group 1 elliptical galaxies. There are, however, at least two ways in which this limit might be circumvented. First, the central regions of elliptical galaxies have very high stellar metallicities, much higher than even the most metal-rich globular clusters (Aaronson et al. 1978). Thus, if there were a stellar component whose X-ray–to–optical luminosity ratio increased extremely rapidly with the metallicity of the stars, then the globular cluster limits would not apply. Since elliptical galaxies have metallicities that decrease with galactocentric radius (Schombert et al. 1993), this model would predict that the X-ray emission in the faintest elliptical galaxies is more centrally condensed than the optical emission. For the X-ray–faint galaxy NGC 4382, the emission in both X-ray bands seems to be somewhat more extended than the optical light. This model would also require that the X-ray colors of group 1 galaxies become harder with increasing radius. For the few group 1 galaxies with enough counts to derive radial color profiles, this does not seem to be the case (see § 6).

Another possible exception to the limits from globular clusters is that they do not apply to any stellar component that is the result of rare but very luminous X-ray sources. Such sources might be too uncommon to have been found in the globular clusters searched. Given the typical blue optical luminosities of the group 1 galaxies of $5.8 \times 10^{10}\ L_{B,\odot}$ and the blue luminosities of the globular clusters of $10^5\ L_{B,\odot}$, such rare sources would have to be more luminous in X-rays than $L_{\rm X} \gtrsim 10^{35}$ ergs s^{-1}. If the X-ray luminosity were less, the number of such objects required in galaxies would imply that one such object would have been observed in most globular clusters observed to date. In fact, one possible candidate (a supersoft source in M3) has been found among all of the globular clusters observed (Verbunt et al. 1995; § 8.3).

8.2. *RS CVn Systems*

RS CVn systems are composed of a G or K giant or subgiant and a late-type main-sequence or subgiant companion. A similar type of binary system is BY Draconis stars, which are composed of two late-type main sequence stars. In principle, these systems have some advantages as X-ray sources in elliptical galaxies when compared to single stars. The rapid rotation brought on by the synchronization of the rotation period to the orbital period leads to substantially higher magnetic activity (and hence X-ray emission) in these systems than in single old main-sequence stars.

Dempsey et al. (1993) find that RS CVn stars have X-ray luminosities that range from 10^{29} to $10^{31.5}$ ergs s^{-1} and spectra that are described by a two-temperature Raymond Smith model: a low-temperature (0.2 keV) component and a high-temperature (1.5 keV) component, with the high-temperature component having a volume emission measure about 2.5 times that of the low-temperature component. Although the presence of a $\sim$0.2 keV component appears promising in explaining the soft component in elliptical and S0 galaxies, the two-temperature model predicts colors of (0.26, 1.51). The C32 color is significantly harder than that observed for group 1 galaxies. Also, the C21 colors of RS CVn stars are also somewhat harder than those observed for the faintest group 1 galaxies, and the addition of a third component needed to lower the C32 value will raise C21 even more. Thus, it appears unlikely that RS CVn systems can contribute appreciably to the X-ray emission of X-ray–faint early-type galaxies. BY Draconis binary systems have nearly identical spectral properties to RS CVn stars (Dempsey et al. 1997) and are also unlikely candidates for the source of the soft X-ray emission in group 1 galaxies.

8.3. *Supersoft Sources*

A relatively new class of X-ray–emitting objects first observed with *Einstein* and later confirmed with *ROSAT* are supersoft sources. Supersoft sources have been detected in our Galaxy (Ögelman et al. 1993), in M31 (Supper et al. 1997), and in the Magellanic Clouds (Kahabka, Pietsch, & Hasinger 1994). Little is known about the distribution and relative number of these sources among Hubble types, so it is possible that early-type galaxies can contain a significantly larger number of them than spiral galaxies. Supersoft sources are characterized by a lack of emission above $\sim$0.4 keV and are believed to be the result of a white dwarf

burning matter accreted from a companion star (van den Heuvel et al. 1992). Supersoft source spectra can be fit by a blackbody model with a temperature of 10–50 eV. They typically have luminosities in the *ROSAT* band of a few times 10^{36} ergs s^{-1} (Kahabka et al. 1994). Thus, $\sim 10^4$ such sources would be necessary to account for the soft X-ray emission in the most X-ray–luminous group 1 galaxies. These sources are bright enough and rare enough that we would not expect them to occur commonly in globular clusters; thus, they would not be subject to the limits on the diffuse soft emission from globular clusters in § 8.1. For a typical globular cluster with an optical luminosity of $L_B \approx 10^5\ L_\odot$, an X-ray–to–optical luminosity ratio of $\log (L_X^h/L_B) = 29.7$ implies an X-ray luminosity of $L_X^s \approx 5 \times 10^{34}$ ergs s^{-1}, or 1/20 of an $L_X^s = 10^{36}$ ergs s^{-1} supersoft source. In fact, only one supersoft source has been observed within a globular cluster; the globular cluster M3 was observed to harbor such a supersoft source (Verbunt et al. 1994), albeit a rather faint one ($L_X \sim 10^{35}$ ergs s^{-1}).

However, the colors predicted by such a component are far too low to match the observed values. A blackbody model with a temperature of 50 eV yields (C21, C32) = (0.005, 0.01). Thus, the addition of supersoft sources will diminish the C21 value obtained for bulges, which is in the opposite sense of what is observed for the brighter group 1 galaxies.

8.4. *Warm Interstellar Gas*

As mentioned above, if the X-ray faintest galaxies have lost their ISM due to winds, there should exist some galaxies that have had some but not all of their ISM removed. The five group 1 galaxies with the highest L_X^h/L_B values may represent this class. Perhaps a few of the faintest group 2 galaxies are members of this class also. The colors of the five group 1 galaxies suspected to have some ISM are (C21, C32) = (0.15–0.30, 0.50–1.0), and the colors of the stellar component as derived from M31 are (C21, C32) = (0.08, 1.15). Depending on the relative contributions from the stellar and gaseous components, the colors of the gaseous component required to yield the observed colors would be in the range (C21, C32) = (0.25–0.50, 0.20–0.85). Judging from the color models of Figure 5, a thermal model with a temperature of 0.3–0.6 keV and a metallicity of 10%–20% of solar would be capable of producing the required colors when combined with the emission from stellar sources. This is the range of temperatures of metallicities that would be expected from interstellar gas in low-luminosity systems, if one extrapolates from the brighter galaxies.

Among the three galaxies for which color profiles could be derived, there is no consensus concerning the radial color trends. NGC 4382 shows a constant C21 and C32 profile. NGC 4697 shows a constant C21 profile and a decreasing C32 profile. NGC 4365 shows a decreasing C21 profile and a constant C32 profile. This lack of agreement could mean that the ISM component is more extended than the stellar component in some galaxies and less extended in others. Alternatively, gradients in the temperature and abundance of the ISM component might also be responsible for the color gradients.

9. CONCLUSIONS

We have analyzed a large elliptical and S0 galaxy sample observed with the *ROSAT* PSPC. We derived X-ray luminosities and X-ray–to–optical luminosity ratios in soft and hard *ROSAT* bands. We defined two X-ray colors; integrated values and radial profiles in these two colors were determined for the galaxies in our sample. We find a very large range in values (a factor of ~ 500) for the X-ray–to–optical luminosity ratio for galaxies in our sample, as has generally been found in the past. The X-ray colors, the color profiles, and the ratio of hard to soft-band luminosities all vary as a function of L_X/L_B, which suggests that different emission processes are important in different galaxies. We divide the galaxies into four groups based on their X-ray–to–optical luminosity ratio: group 1, $\log (L_X^h/L_B) < 29.7$; group 2, $29.7 \leq \log (L_X^h/L_B) < 30.0$; group 3, $30.0 \leq \log (L_X^h/L_B) < 30.4$; and group 4, $\log (L_X^h/L_B) \geq 30.4$.

The X-ray brightest galaxies (group 4) have colors and luminosities that are consistent with thermal emission from hot gas at temperatures around 0.8 keV and abundances of approximately one-half solar. These galaxies have hard and soft-band X-ray luminosities that increase in proportion to one another and that increase rapidly with the optical luminosity. They often sit at the centers of groups, and there is evidence that this increases their X-ray luminosities. The galaxies in deeper potential wells may have higher X-ray luminosities per unit blue luminosity because they have lost less gas during their early evolution or have accreted group gas.

The intermediate X-ray luminosity galaxies (groups 2 and 3) have colors that are generally consistent with thermal emission from lower temperature and abundance gas than the group 4 galaxies. For these galaxies, the soft-band X-ray luminosity–to–optical luminosity ratios (L_X^s/L_B) are nearly constant from galaxy to galaxy, while the hard-band luminosity drops more rapidly than the optical luminosity. One explanation for this trend would be if the hard-band luminosity were dominated by thermal emission by gas and the soft-band luminosity were dominated by stellar sources. This would require that the thermal X-ray luminosity decline rapidly with decreasing optical luminosity, as is seen for the brighter group 1 galaxies. However, this would not explain why the soft-band X-ray–to–optical luminosity ratio, L_X^s/L_B, continues to decrease for $\log (L_X^h/L_B) \lesssim 29.7$. Also, the *ROSAT* and *ASCA* X-ray spectra of these galaxies suggest that the bulk of the emission is thermal emission from hot gas with subsolar abundances (e.g., Davis & White 1996; Matsumoto et al. 1997). Alternatively, the bulk of the X-ray luminosity might be thermal in origin, with L_X^h/L_B decreasing as the gaseous iron abundance decreases. We show that lowering the iron abundance mainly reduces the *ROSAT* hard-band emission because this emission is dominated by the iron *L*-line complex at ~ 1 keV.

The X-ray emission from most of the fainter group 1 galaxies can best be described as the integrated emission from low-mass X-ray binaries, as was seen to be the case for the bulge of M31. In these galaxies, the ISM could have been removed by supernovae-driven winds. The X-ray colors and X-ray–to–optical luminosity ratios for all but a small subset of the group 1 galaxies were consistent with the colors of the bulges of M31 and NGC 1291. The soft component previously seen in these galaxies was shown to be the result of the more complex spectrum of LMXBs; they are not well represented by a simple, single-temperature 5 keV bremsstrahlung model, which had been previously assumed for LMXBs. The X-ray colors of the nearby LMXB Her X-1 confirm the existence of a soft X-ray com-

ponent in at least one Galactic LMXB. Individual LMXBs in the faintest galaxies should be resolvable with *AXAF* for galaxies as far away as Virgo.

As supporting evidence that the soft component is from LMXBs, we show that the three most likely alternative stellar sources of the soft emission are unlikely to be important contributors. We find that M stars can match the X-ray colors of group 1 elliptical galaxies but that they are probably too faint. We set a limit on the cumulative X-ray luminosity of old M stars from upper limits on the diffuse X-ray emission from globular clusters. This gives X-ray luminosities that are a factor of at least 300 lower than the soft-band X-ray luminosities of group 1 elliptical galaxies. (However, this limit might not apply if the X-ray emission from M stars increased strongly with metallicity.) RS CVn stars have C32 colors that are too hard to match the observed colors of elliptical galaxies, and adding hard emission from LMXBs only increases the discrepancy. Supersoft sources are too soft to explain the observed colors of elliptical galaxies.

The brightest of the group 1 galaxies might contain significant amounts of interstellar matter that has not been completely removed from the galaxy. These galaxies have higher C21 values and lower C32 values than the other group 1 galaxies. This would account for their higher L_X/L_B values as compared to the faintest group 1 galaxies and the bulges. If the ISM has a temperature of 0.3–0.6 keV and low metallicities, its emission would produce the observed colors when mixed with the right proportion of stellar emission.

Finally, we find that the faintest X-ray galaxies have hard-band *ROSAT* X-ray luminosities that are significantly less than expected from the integrated emission of LMXBs, as derived from brighter elliptical galaxies (Matsumoto et al. 1997) and spiral galaxy bulges. This suggests that the fractional population or luminosity of LMXBs may be lower in less luminous galaxies. One way to produce such a variation would be if the slope of the initial mass function in early-type galaxies became flatter as the optical luminosity increased. Small-number statistical variations in the number of LMXBs in these galaxies may also play a role.

We thank Michael Loewenstein and an anonymous referee for many very useful comments and suggestions. We also thank Steve Balbus, Tim Kallman, Bob O'Connell, Richard Mushotzky, and Jean Swank for useful discussions. This research has made use of data obtained through the High Energy Astrophysics Science Archive Research Center Online Service, provided by the NASA/Goddard Space Flight Center. J. A. I. and C. L. S. were supported in part by NASA *ROSAT* grant NAG 5-3308 and *ASCA* grant NAG 5-2526. C. L. S. was also supported by NASA Astrophysical Theory Program grant 5-3057. J. A. I. was supported by the Achievement Rewards for College Scientists Fellowship, Metropolitan Washington Chapter.

REFERENCES

Aaronson, M., Cohen, J. G., Mould, J., & Malkan, M. 1978, ApJ, 223, 824
Arimoto, N., Matsushita, K., Ishimaru, Y., Ohashi, T., & Renzini, A. 1997, ApJ, 477, 128
Bregman, J. N., Hogg, D. E., & Roberts, M. S. 1995, ApJ, 441, 561
Buote, D. A., & Canizares, C. R. 1994, ApJ, 427, 86
———. 1997, ApJ, 474, 650
Canizares, C. R., Fabbiano, G., & Trinchieri, G. 1987, ApJ, 312, 503
Choi, C. S., Seon, K. I., Dotani, T., & Nagase, F. 1996, ApJ, 476, L81
Ciotti, L., Pellegrini, S., Renzini, A., & D'Ercole, A. 1991, ApJ, 376, 380
David, L. P., Forman, W., & Jones, C. 1991, ApJ, 369, 121
Davis, D. S., & White, R. E., III. 1996, ApJ, 470, L35
Dempsey, R. C., Linsky, J. L., Fleming, T. A., & Schmitt, J. H. M. M. 1997, ApJ, 478, 358
Dempsey, R. C., Linsky, J. L., Schmitt, J. H. M. M., & Fleming, T. A. 1993, ApJ, 413, 333
de Vaucouleurs, G. 1975, ApJS, 29, 193
de Vaucouleurs, G., et al. 1991, Third Reference Catalogue of Bright Galaxies (New York: Springer)
Eskridge, P. B., White, R. E., III, & Davis, D. S. 1996, ApJ, 463, L59
Fabbiano, G., Kim, D.-W., & Trinchieri, G. 1992, ApJS, 80, 531
———. 1994, ApJ, 429, 94
Fabbiano, G., Trinchieri, G., & Van Speybroeck, L. S. 1987, ApJ, 316, 127
Faber, S. M., Wegner, G., Burstein, D., Davies, R. L., Dressler, A., Lynden-Bell, D., & Terlevich, R. J. 1989, ApJS, 69, 763
Forman, W., Jones, C., David, L., Franx, M., Makishima, K., & Ohashi, T. 1993, ApJ, 418, L55
Forman, W., Jones, C., & Tucker, W. C. 1985, ApJ, 293, 102
Forman, W., Schwarz, J., Jones, C., Liller, W., & Fabian, A. C. 1979, ApJ, 234, L27
Giampapa, M. S., Rosner, R., Kashyap, V., Fleming, T. A., Schmitt, J. H. M. M., & Bookbinder, J. A. 1996, ApJ, 463, 707
Isobe, T., Feigelson, E. D., & Nelson, P. I. 1986, ApJ, 306, 490
Kahabka, P., Pietsch, W., & Hasinger, G. 1994, A&A, 288, 538
Kim, D.-W., & Fabbiano, G. 1995, ApJ, 441, 182
Kim, D.-W., Fabbiano, G., Matsumoto, H., Koyama, K., & Trinchieri, G. 1996, ApJ, 468, 175
Kim, D.-W., Fabbiano, G., & Trinchieri, G. 1992, ApJ, 393, 134
Loewenstein, M. 1996, in Cosmic Abundances, ed. S. Holt & G. Sonneborn (San Francisco: ASP), 393
Loewenstein, M., & Mathews, W. G. 1987, ApJ, 319, 614
Matsumoto, H., Koyama, K., Awaki, H., Tsuru, T., Loewenstein, M., & Matsushita, K. 1997, ApJ, 482, 133
Mushotzky, R. F., Loewenstein, M., Awaki, H., Makishima, K., & Matsumoto, H. 1994, ApJ, 436, L79
Matteucci, F. 1994, A&A, 288, 57
Mavromatakis, F. 1993, A&A, 273, 147
Ögelman, H., Orio, M., Krautter, J., & Starrfield, S. 1993, Nature, 361, 331
Pellegrini, S. 1994, A&A, 292, 395
Pellegrini, S., & Fabbiano, G. 1994, ApJ, 429, 105
Peterson, C. J. 1993, in Structure and Dynamics of Globular Clusters, ed. S. G. Djorgovski & G. Meylan (San Francisco: ASP), 337
Raymond, J. C., & Smith, B. W. 1977, ApJS, 35, 419
Sadler, E. M., Jenkins, C. R., & Kotanyi, C. G. 1989, MNRAS, 240, 591
Schmitt, J. H. M. M., Fleming, T. A., & Giampapa, M. S. 1995, ApJ, 450, 392
Schombert, J. M., Hanlan, P. C., Barsony, M., & Rakos, K. D. 1993, AJ, 106, 923
Skumanich, A. 1972, ApJ, 171, 565
Snowden, S. L. 1995, Cookbook for Analysis Procedures for *ROSAT* XRT/PSPC Observations of Extended Objects and the Diffuse Background (Greenbelt, MD: GSFC)
Stark, A. A., Gammie, C. F., Wilson, R. W., Bally, J., Linke, R. A., Heiles, C., & Hurwitz, M. 1992, ApJS, 79, 77
Supper, R., Hasinger, G., Pietsch, W., Trümper, J., Jain, A., Magnier, E. A., Lewin, W. H. G., & van Paradijs, J. 1997, A&A, 317, 328
Trager, S. C., Djorgovski, S., & King, I. R. 1993, in ASP Conf. Proc. 50, Structure and Dynamics of Globular Clusters, ed. S. G. Djorgovski and G. Meylan, (San Francisco: ASP), 347
Trinchieri, G., & Fabbiano, G. 1985, ApJ, 296, 447
Trinchieri, G., Kim, D.-W., Fabbiano, G., & Canizares, C. R. 1994, ApJ, 428, 555
Tully, B. R. 1988, Nearby Galaxies Catalog (New York: Cambridge Univ. Press)
van den Heuvel, E. P. J., Bhattacharya, D., Nomoto, K., & Rappaport, S. A. 1992, A&A, 262, 97
Verbunt, F., Bunk, W., Hasinger, G., & Johnston, H. 1995, A&A, 300, 732
Veron-Cetty, M. P., & Veron, P. 1996, A Catalogue of Quasars and Active Nuclei (ESO Scientific Report 17) (7th ed.; Garching bei München: ESO)
Vrtilek, S. D., et al. 1994, ApJ, 436, L9
Walterbos, R. A. M., & Kennicutt, R. C. 1988, A&A, 198, 61
White, R. E., III, & Davis, D. S. 1997, in ASP Conf. Proc. 115, Galactic and Cluster Cooling Flows, ed. N. Soker (San Francisco: ASP), 217
Worthey, G., Faber, S. M., & Gonzalez, J. J. 1992, ApJ, 398, 69